SAND2015-4936PE

Exceptional service in the national interest

Sandia National Laboratories

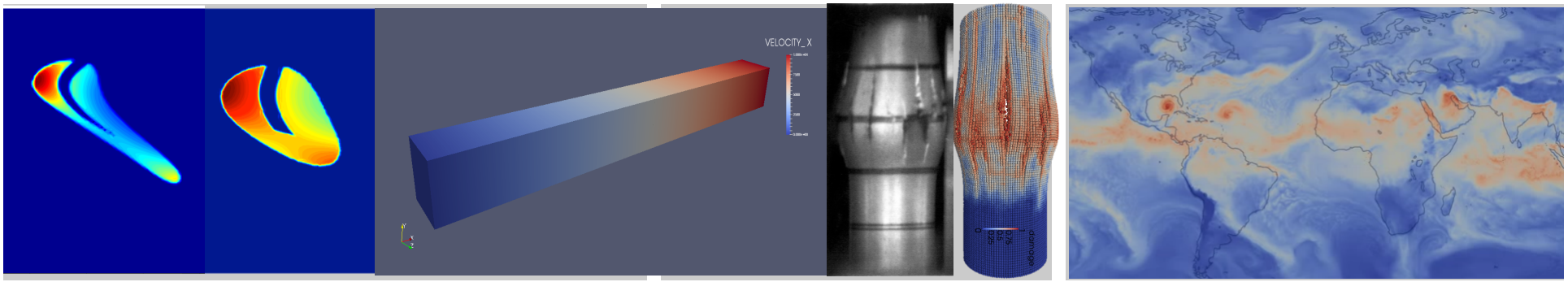

Optimization-Based Property Preserving Methods, or

Going Boldly Beyond Compatible Discretizations

CCR Center for Computing Research

Pavel Bochev
Sandia National Laboratories

U.S. DEPARTMENT OF ENERGY | Office of Science

Collaboratory on Mathematics for Mesoscopic Modeling of Materials (CM4)

U.S. DEPARTMENT OF ENERGY | NNSA National Nuclear Security Administration | ASC

New trends in compatible discretizations

CEA-EDF-INRIA School, June 29 - July, 02, 2015 INRIA Paris-Rocquencourt

Sandia National Laboratories is a multi-program laboratory managed and operated by Sandia Corporation, a wholly owned subsidiary of Lockheed Martin Corporation, for the U.S. Department of Energy's National Nuclear Security Administration under contract DE-AC04-94AL85000. SAND NO. 2011-XXXXP

Roadmap

Sandia National Laboratories

- **Prologue**
  - What do we want in a numerical method?
  - What are the challenges?
  - What do we propose to do: an overview of optimization ideas
- **Case study 1: Optimization-based Heterogeneous Numerical Methods**
  - Application to the coupling of local and nonlocal models
- **Case study 2: Optimization-based transport schemes**
  - A spectral element scheme
  - A cell-centered scheme

Thanks to:

- M. D'Elia, P. Kuberry, D. Littlewood, M. Perego, K. Peterson, D. Ridzal (SNL)
- M. Shashkov (LANL)
- M. Gunzburger (FSU), A. Shapeev (SkolTech), S.Moe (U. WA),
- M. Luskin, D. Olson (U. MN)

What do we want?

- **DOE uses computer models** to understand, predict, and verify complex systems in **high consequences analyses** that would be difficult or even impossible by other means.
- **Integrated models** of such systems incorporate **diverse "mathematical parts"**: *PDEs, non-local (integral) equations, classical DFT, potential-based atomistic* and so on…

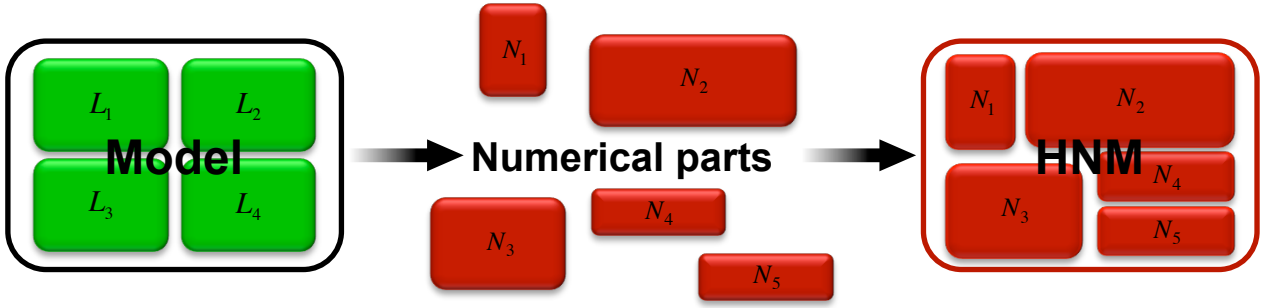

HNM = Collection of dissimilar numerical models from multiple disciplines functioning together as a unified simulation tool

- **Diversity of models leads to a diversity of "numerical parts":** mesh based (FE, FV, FD), particle based (SPH, DPD, MLS), implicit, explicit, Eulerian, Lagrangian, semi-Lagranian…
- **Requirements[1]:**
  - Each part must be **stable**, **accurate** and **preserve the relevant physical properties.**
  - The parts must function together as a **unified simulation tool.**
  - This tool itself must be **stable, accurate** and **preserve the relevant physical properties.**

[1] Of course, we also need efficient solvers, but this is beyond the scope of this talk

What are the challenges?

Sandia National Laboratories

1. Achieving Stability & Accuracy (Structural aspects)

- **Game changer**: Homological techniques: FE exterior calculus (DEC), mimetic FD,…
- Typically achieved by *topological means:*
  - Careful placement of the variables on the mesh;
  - Special grid structure, e.g., topologically dual grids
- **Challenges**:
  1. **Models that don't fit EC structure**, e.g., heterogeneous methods: FEM+SPH
  2. **Stable and accurate** does not imply **property preserving**…

2. Preserving Physical Properties (Qualitative aspects)

- Maximum principles, local bounds, symmetries, Geometric Conservation Laws,…
- Correlations between variables, e.g., between two passive tracers.
- **Challenges**: conventional ways to preserve these properties are either
  - **Restrictive**: Cartesian mesh, angle conditions, etc, and/or,
  - **Entangle accuracy** with the property preservation, e.g., limiters.
- **Game changer**? **Optimization!**

What are the challenges?

Sandia National Laboratories

3. Assembling Diverse Numerical Parts into HNMs

☞"Exascale computing will enable consideration of new classes of multiscale problems in which different types of discretizations, appropriate to a particular scale in different portions of the domain, are employed and models which treat distinct phenomena in different parts of the domain, such as ocean-atmosphere coupling…"

☞"Effective models must be hierarchical and include multiple sub-models that represent different phenomena with vastly differing scales."

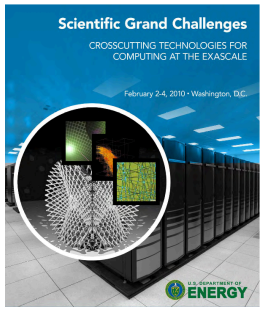

"As this type of simulation expands, there is a critical need to develop systematic approaches for coupling across the range of scales and quantification of the properties of these types of coupling strategies"

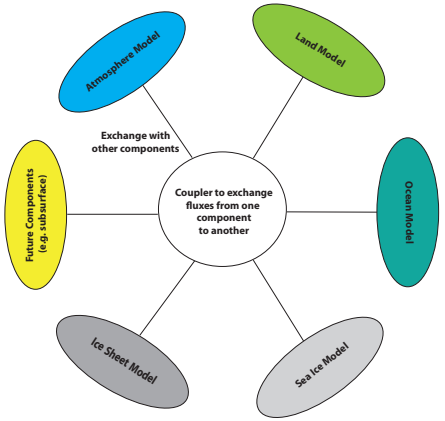

Global Earth System Model

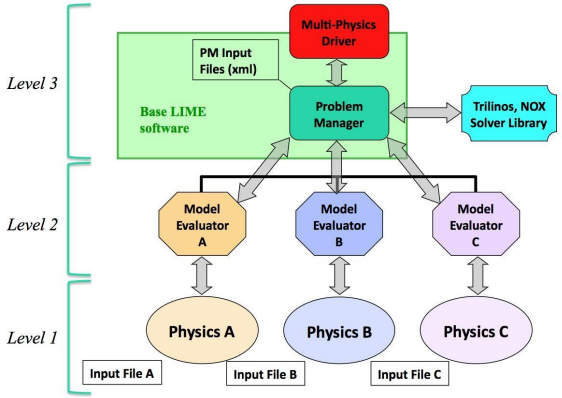

LIME: Lightweight Integrating Multiphysics Environment (CASL)

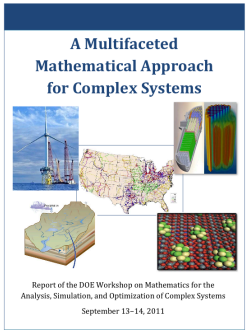

Traditional monolithic and operator-splitting modeling approaches fall short of meeting the crosscutting challenges; see *Multifaceted Mathematical Approach for Complex Systems.*

What do we propose to do

Couch assembly of numerical parts and preservation of properties into an optimization problem:

Minimize

Coupling mismatch $\left\| u_1^h - u_2^h \right\|^2$ + $\sum_{i=1,2} \left\| u_i^h - u_i^T \right\|^2$ **Target mismatch**

Subject to

Component physics $L_1^h(u_1^h, \theta) = f_1$ $\quad$ $\underline{C}_i \le C u_i^h \le \overline{C}_i$ $\quad$ **Physical properties**

$L_2^h(u_2^h, \theta) = f_2$ $\quad$ $B u_i^h = b$

- **Reverses the roles** of the coupling conditions and the models
- **Divide and conquer approach:**
  - **separates numerical parts: facilitates merging of heterogeneous methods**
  - **separates *accuracy* from *physical properties*** (local bounds, conservation, etc..)

Sandia National Laboratories

Part 1

Case study 1: optimization-based HNMs

Sandia National Laboratories

In Part 1 we consider HNMs combining local (PDE) and non-local models. Such couplings are often called heterogeneous domain decomposition.

Minimize

Coupling mismatch $\left\| u_1^h - u_2^h \right\|^2$ + $\sum_i \left\| u_i^h - u_i^T \right\|^2$ **Target mismatch**

Subject to

Component physics $L_1^h(u_1^h, \theta) = f_1$

$L_2^h(u_2^h, \theta) = f_2$

$\underline{C}_i \le C u_i^h \le \overline{C}_i$ **Physical properties**

$B u_i^h = b$

This case study highlights the use of optimization ideas for the stable and accurate coupling of fundamentally different numerical models.

Related work: Lions (2001), Quarteroni (2000), Gunzburger (2000), Du (2001) – applications to PDEs, Oden (2011 – Atomistic to Continuum), Discacciati (2013 – heterogeneous domain decomposition), Karniadakis (2014-Stochastic PDE)

Why Local-to-Nonlocal (LtN) couplings?

Sandia National Laboratories

- **Nonlocal continuum mechanics**: **allows interactions at distance without contact:**
  - Can accurately resolve small scale features, e.g., crack tips or dislocations.

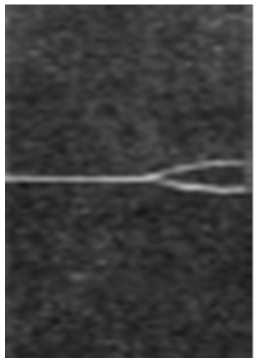

- **Nonlocal dielectric models**: **more accurate description of solvation processes:**
  - Essential in, e.g., electrokinetic nanofluidic channels, where local response modification to Poisson-Boltzmann are qualitatively incorrect.
- **Atomistic models: accurate simulation of defects (vacancy, impurity…)**
- **Classical DFT**: **evaluation of chemical potentials of charged species**
  - More accurate than Poisson-Nernst-Planck models at mesoscale.

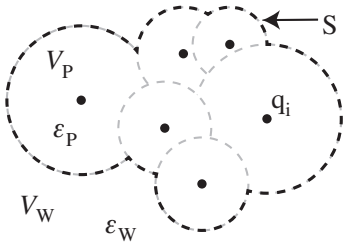

However, full nonlocal simulation can be very expensive!

Coupling to local (PDE) models can improve efficiency.

Anatase TiO_2 nanoparticles in DI water + HCl to control pH

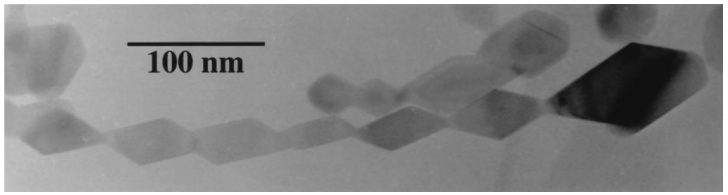

Penn, Banfield. Geochim. et Cosmochim. Acta, 63/10, 1999

J. Bardhan. "Gradient models in molecular biophysics: Progress, challenges, opportunities.". Journal of the mechanical behavior of materials, 22.5-6: 2013

R. Nilson and S. Griffiths. Influence of atomistic physics on electro-osmotic flow: An analysis based on DFT. The Journal of Chemical Physics, 125(16), 2006.

A non-overlapping LtN example

Sandia National Laboratories

Expanding tube experiment

- Tube expansion via collision of Lexan projectile and plug within AerMet tube
- Accurate recording of velocity and displacement on tube surface

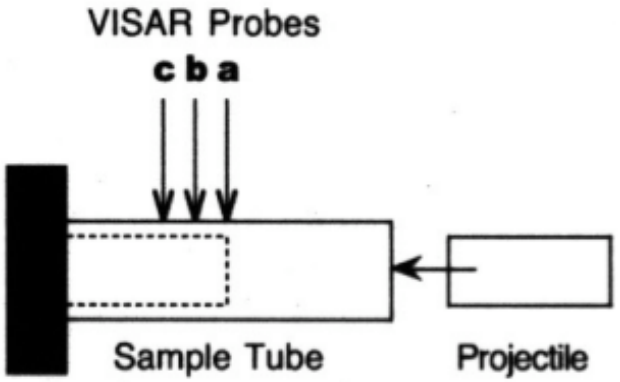

Experimental setup*

Modeling Approach

- AerMet tube: **nonlocal peridynamics**, elastic-plastic material model with linear hardening
- Lexan plugs: **classical local (PDE)**, equation-of-state Johnson-Cook material model
- Interaction via **contact algorithm**

Discretization

- Particles (Perydigm) + nodal FEM (Sierra/SM)
- Contact algorithm.

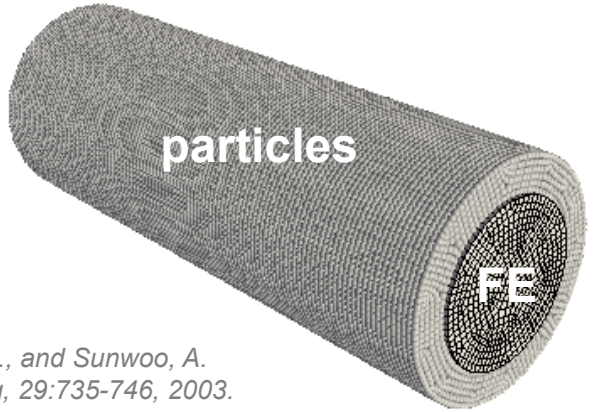

** Vogler, T.J., Thornhill, T.F., Reinhart, W.D., Chhabidas, L.C., Grady, D.E., Wilson, L.T., Hurricane, O.A., and Sunwoo, A. Fragmentation of materials in expanding tube experiments. International Journal of Impact Engineering, 29:735-746, 2003.*

*** D. Littlewood. 2010. Simulation of dynamic fracture using peridynamics, finite element modeling, and contact. Proceedings of the ASME 2010 International Mechanical Engineering Congress and Exposition, British Columbia, Canada.*

Expanding tube simulation

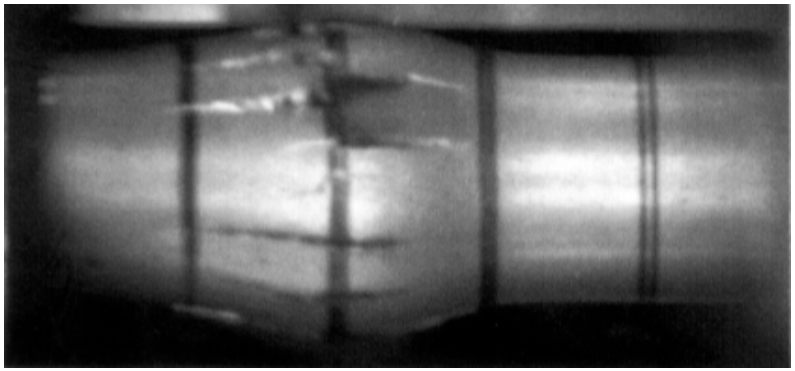

Experimental image at 15.4 microseconds*

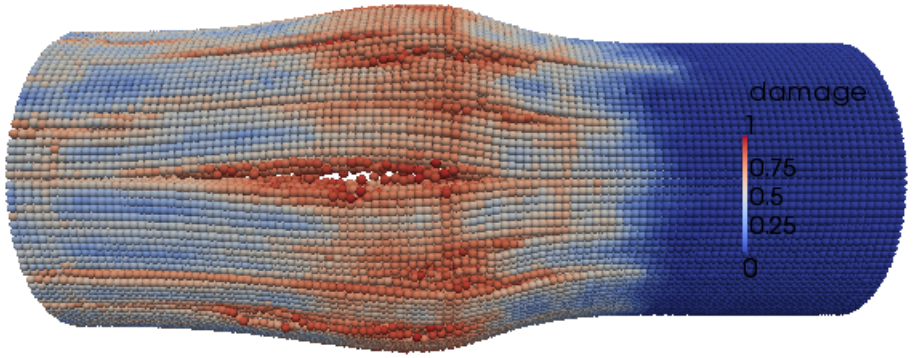

Simulation at 15.4 microseconds**

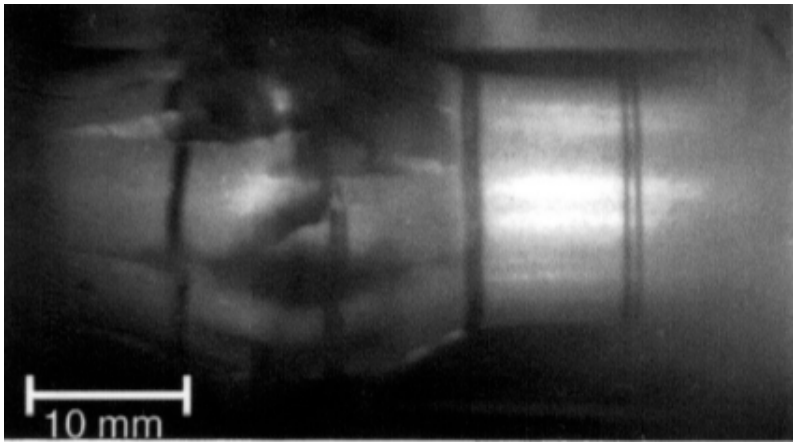

Experimental image at 23.4 microseconds*

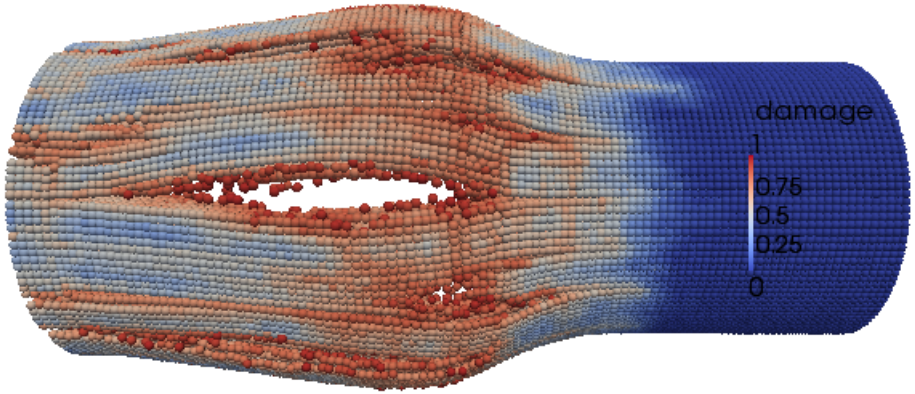

Simulation at 23.4 microseconds**

** Vogler, T.J., Thornhill, T.F., Reinhart, W.D., Chhabidas, L.C., Grady, D.E., Wilson, L.T., Hurricane, O.A., and Sunwoo, A. Fragmentation of materials in expanding tube experiments. International Journal of Impact Engineering, 29:735-746, 2003.*

*** D. Littlewood. 2010. Simulation of dynamic fracture using peridynamics, finite element modeling, and contact. Proceedings of the ASME 2010 International Mechanical Engineering Congress and Exposition, British Columbia, Canada.*

Expanding tube simulation

Displacement and velocity
on tube surface
at probe position (**a**)

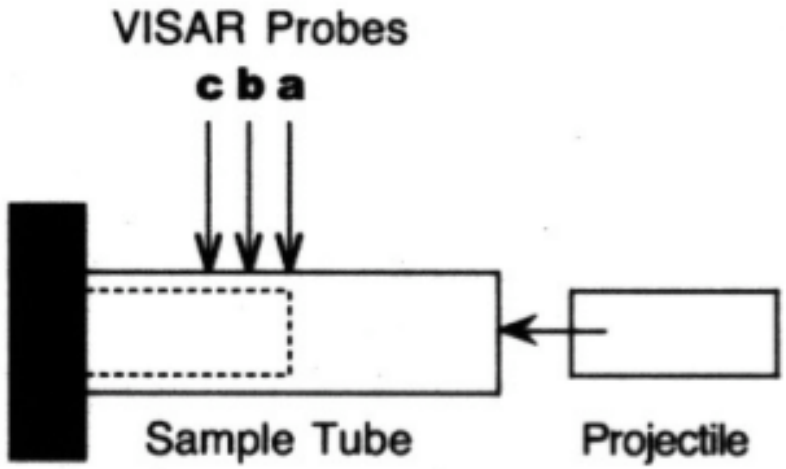

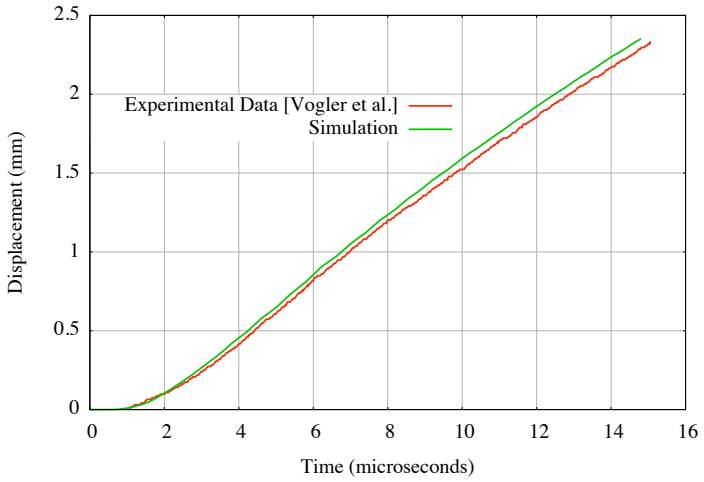

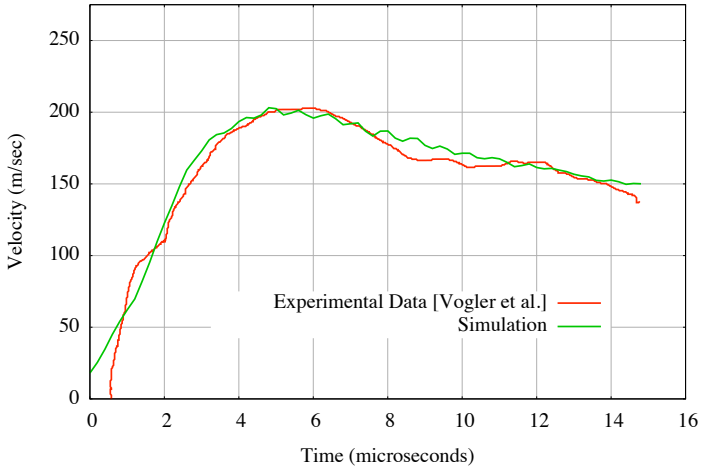

** Vogler, T.J., Thornhill, T.F., Reinhart, W.D., Chhabidas, L.C., Grady, D.E., Wilson, L.T., Hurricane, O.A., and Sunwoo, A. Fragmentation of materials in expanding tube experiments. International Journal of Impact Engineering, 29:735-746, 2003.*

*** D. Littlewood. 2010. Simulation of dynamic fracture using peridynamics, finite element modeling, and contact. Proceedings of the ASME 2010 International Mechanical Engineering Congress and Exposition, British Columbia, Canada.*

An optimization based LtN coupling

Sandia National Laboratories

The nonlocal problem

$$\begin{cases} -\mathcal{L}u_n &= f_n \quad \boldsymbol{x} \in \Omega \\ u_n &= \sigma_n \quad \boldsymbol{x} \in \widetilde{\Omega}, \end{cases}$$

The nonlocal diffusion operator

$$\mathcal{L}u(\boldsymbol{x}) = \int_{\mathbb{R}^n} \big(u(\boldsymbol{y}) - u(\boldsymbol{x})\big)\, \gamma(\boldsymbol{x}, \boldsymbol{y})\, d\boldsymbol{y}$$

acting on $u(\boldsymbol{x}) \colon \mathbb{R}^d \to \mathbb{R}$

The local problem

local diffusion model given by the Poisson equation

$$\begin{cases} -\Delta u_l &= f_l \quad \boldsymbol{x} \in \Omega \\ u_l &= \sigma_l \quad \boldsymbol{x} \in \partial\Omega, \end{cases}$$

where $\sigma_l \in H^{\frac{1}{2}}(\partial\Omega)$ and $f_l \in L^2(\Omega)$

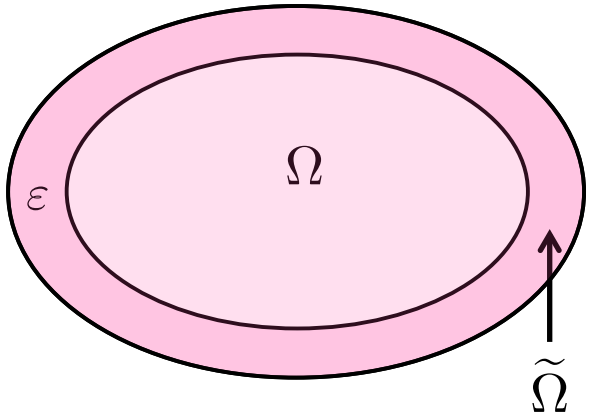

- *D'Elia, Bochev, Mat. Res. Soc. Cambridge Univ. Pres. 2015.*
- *D'Elia, Bochev, SIAM J. Num. Anal. 2015 (submitted).*

Optimization-based LtN formulation

We couch the LtN coupling into a constrained optimization problem:

$$\min_{u_n,u_l,\theta_n,\theta_l} J(u_n,u_l)=\frac{1}{2}\|u_n-u_l\|^2_{0,\Omega_b} \quad \text{s.t.}$$

Nonlocal

$$\begin{cases} -\mathcal{L}u_n = f_n & \boldsymbol{x}\in\Omega_n \\ u_n = \theta_n & \boldsymbol{x}\in\widetilde{\Omega}_c \\ u_n = 0 & \boldsymbol{x}\in\widetilde{\Omega}_i \end{cases}$$

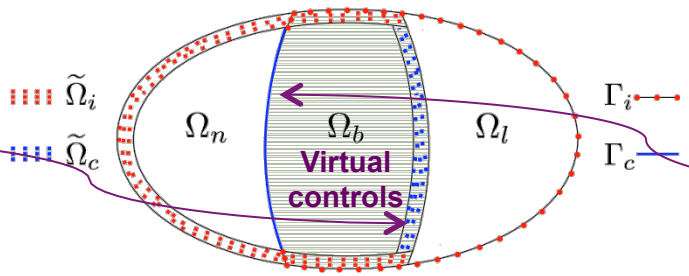

Local

$$\begin{cases} -\Delta u_l = f_l & \boldsymbol{x}\in\Omega_l \\ u_l = \theta_l & \boldsymbol{x}\in\Gamma_c \\ u_l = 0 & \boldsymbol{x}\in\Gamma_i. \end{cases}$$

CM4, ASCR

Key properties of the optimization-based LtN formulation:

- Eliminates ghost forces and is consistent for all polynomial orders.
- Is provably stable & admits rigorous coupling and discretization error analysis.
- Basic idea applicable to diverse modeling scenarios:
  - PNP+cDFT, local+nonlocal dielectric, Atomistic-to-Continuum coupling.,…

*None of the existing multi-model coupling formulations such as **Arlequin**, **blending**, **morphing**, **force-based**, etc. **possess all of these properties**!*

Optimization vs. traditional couplings

Sandia National Laboratories

An example of an energy-blended LtN method

$$\begin{cases} \text{minimize} \quad E_N(\sqrt{\alpha}u_N) + E_L(\sqrt{(1-\alpha)}u_L) \\ \text{subject to} \quad \|\Pi u_N - u_L\|_{\Omega_o} = 0 \end{cases}$$

Bauman et al, Comp. Mech. (2008) 42.

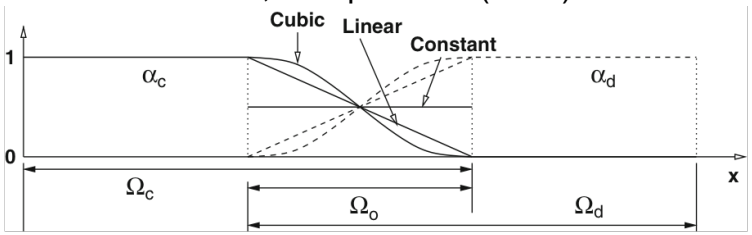

Minimize blended energy subject to constraints **forcing the equality of the nonlocal and local states**

- Blending of two disparate physical models is **mathematically challenging**
- The notion of "equality" depends on the projection **Π,** introducing **some ambiguity**
- Resulting LtN formulations may suffer from spurious effects, e.g., **ghost forces**

An optimization-based LtN approach: reverse the roles!

Minimize the mismatch between the nonlocal and local states subject to the **two models acting independently** in Ω_N and Ω_L

Existence of an optimal solution

Sandia National Laboratories

Reduced space formulation

We switch to an equivalent **reduced space problem** in terms of the virtual controls only

$$\begin{cases} -\mathcal{L}u_n = f_n & \text{in } \Omega_n \\ u_n = \theta_n & \text{on } \tilde{\Omega}_c \\ u_n = 0 & \text{on } \tilde{\Omega}_i \end{cases} \rightarrow \quad u_n = u_n(\theta_n)$$

$$\begin{cases} -\Delta u_l = f_l & \text{in } \Omega_l \\ u_l = \theta_l & \text{on } \Gamma_c \\ u_l = 0 & \text{on } \Gamma_i \end{cases} \rightarrow \quad u_l = u_l(\theta_l)$$

$$\underset{\Lambda_n \times \Lambda_l}{\text{minimize}} \ \frac{1}{2}\left\| u_n(\theta_n) - u_l(\theta_l) \right\|^2_{0,\Omega_b}$$

Unconstrained minimization problem over the nonlocal and local trace spaces Λ_n and Λ_l

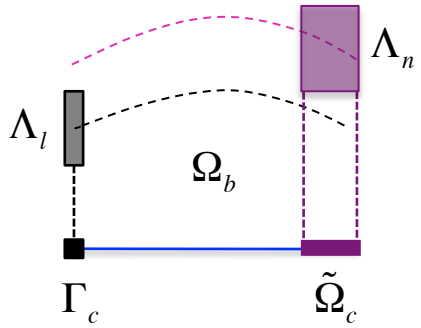

Existence of an optimal solution

Decomposition of the states into harmonic and homogeneous parts:

$$u_n(\theta_n) = v_n(\theta_n) + u_n^0 \longrightarrow \begin{cases} -\mathcal{L} v_n = 0 & \text{in } \Omega_n \\ v_n = \theta_n & \text{on } \tilde{\Omega}_c \end{cases} \quad \begin{cases} -\mathcal{L} u_n^0 = f_n & \text{in } \Omega_n \\ u_n^0 = 0 & \text{on } \tilde{\Omega}_n \end{cases} \longrightarrow$$

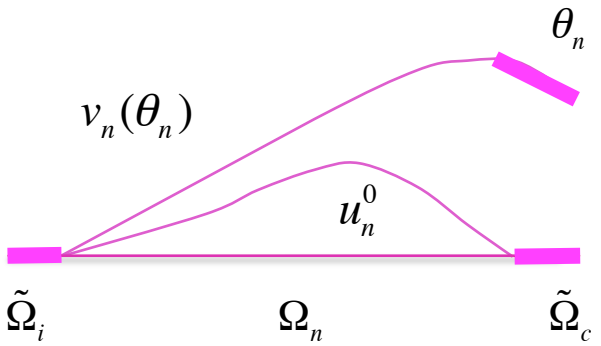

$$u_l(\theta_l) = v_l(\theta_l) + u_l^0 \longrightarrow \begin{cases} -\Delta v_l = 0 & \text{in } \Omega_l \\ v_l = \theta_l & \text{on } \Gamma_c \end{cases} \quad \begin{cases} -\Delta u_l^0 = f_l & \text{in } \Omega_l \\ u_l^0 = 0 & \text{on } \Gamma_l \end{cases} \longrightarrow$$

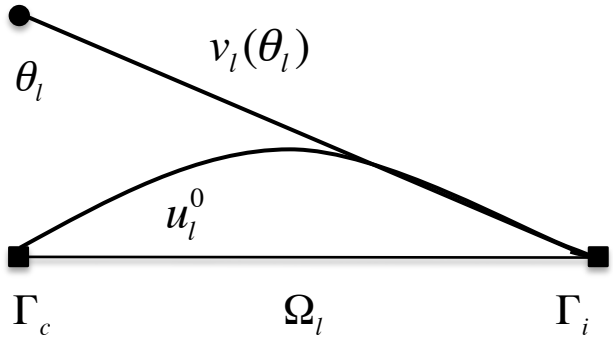

This decomposition follows the idea of Gervasio et al., Num. Math. 2001

Existence of an optimal solution

Sandia National Laboratories

Reduced space problem in terms of the dual norm

$$\underset{\Lambda_n \times \Lambda_l}{\text{minimize}} \ \frac{1}{2}\left\|\{\theta_n,\theta_l\}\right\|_*^2 + \left(v_n(\theta_n) - v_l(\theta_l), u_n^0 - u_l^0\right)_{0,\Omega_b} + \frac{1}{2}\left\|u_n^0 - u_l^0\right\|_{0,\Omega_b}$$

The corresponding Euler-Lagrange equation

$$\left\langle \{\theta_n,\theta_l\},\{\mu_n,\mu_l\}\right\rangle_* = -\left(u_n^0 - u_l^0, v_n(\mu_n) - v_l(\mu_l)\right)_{0,\Omega_b} \quad \forall \{\mu_n,\mu_n\} \in \Lambda_n \times \Lambda_l$$

Theorem

The following form defines an inner product on the trace space $\Lambda_n \times \Lambda_l$.

$$\left\langle \{\theta_n,\theta_l\},\{\mu_n,\mu_l\}\right\rangle_* := \left(v_n(\theta_n) - v_l(\theta_l), v_n(\mu_n) - v_l(\mu_l)\right)_{0,\Omega_b}$$

Corollary. The reduced space problem has a unique solution $\{\theta_n,\theta_l\} \in \Lambda_n \times \Lambda_l$.

The LtN approximation

Solution procedure

1. Solve the reduced space problem:

$$\left\{\theta_n^*, \theta_l^*\right\} \in \Lambda_n \times \Lambda_l$$

approximate solution traces →

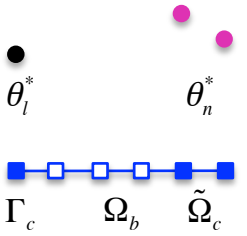

2. Recover the optimal states

$$u_n^* = u_n^0 + v_n(\theta_n^*) \quad \text{and} \quad u_l^* = u_l^0 + v_l(\theta_l^*)$$

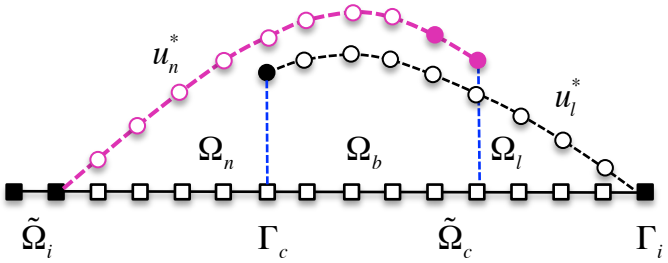

3. Stitch them into an LtN solution

$$u^* = \begin{cases} u_n^* & \text{in } \Omega_n^+ \\ u_l^* & \text{in } \Omega_l \setminus \Omega_b \end{cases}$$

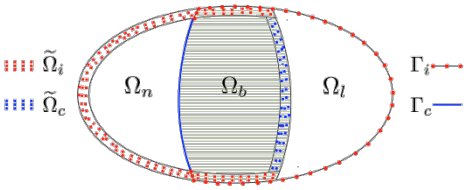

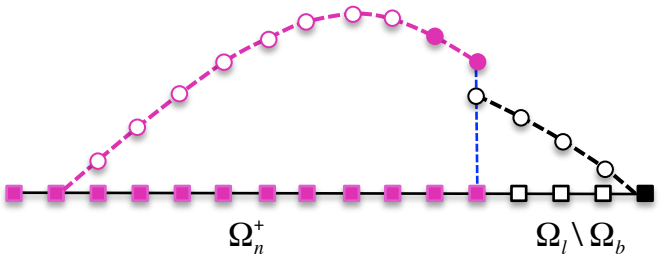

Analysis of the LtN coupling error

Sandia National Laboratories

Assumptions

- The global non-local solution $\hat{u}_n$ has a well-defined trace on Γ_c:

$$T(u) = \left(T_n(u), T_l(u)\right) = \left(u|_{\tilde{\Omega}_c}, u|_{\Gamma_c}\right)$$

- The kernel $\gamma(x,y)$ is such that

$$\overline{\gamma}_k < \infty \quad where \quad \overline{\gamma}_k = \|\gamma_k\|_{\infty,\Omega}^{1/k}, \quad \gamma_k = \int_{\Omega^+} \gamma^k(x,y)\,dy$$

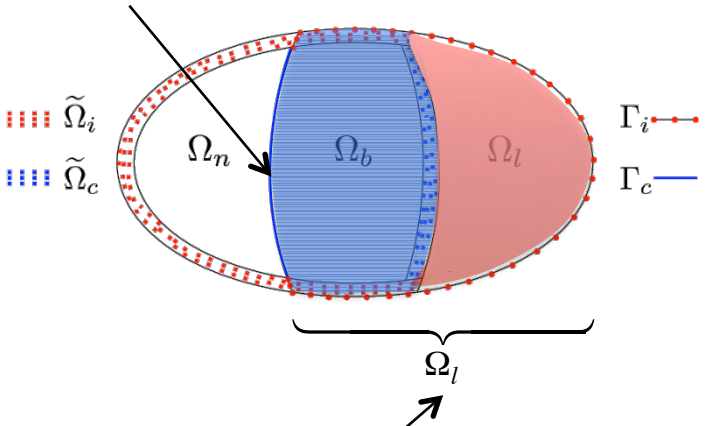

Main result

Theorem

LtN **coupling error** is bounded by the **modeling error** on the **local subdomain**:

$$\left\|\hat{u}_n - u^*\right\|_{0,\Omega^+} \le (1 + C(\Omega_b))\left\|\hat{u}_n - \hat{u}_l\right\|_{0,\Omega_l}$$

where $\hat{u}_n$ - global nonlocal and

$$\begin{cases} -\Delta\hat{u}_l = f & \text{in } \Omega_l \\ \hat{u}_l = T_l(\hat{u}_n) & \text{on } \Gamma_c \\ \hat{u}_l = 0 & \text{on } \Gamma_i \end{cases}$$

Elements of the proof

Sandia National Laboratories

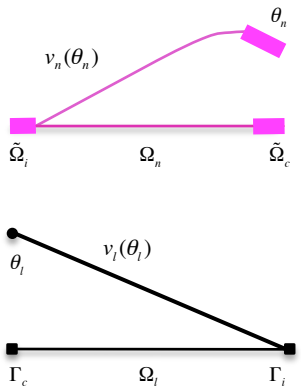

Harmonic lifting operator

$$L(\mu_n,\mu_l)=\mathbf{u}^0+H(\mu_n,\mu_l) \quad \text{where} \quad \mathbf{u}^0=\begin{pmatrix}u_n^0\\ u_l^0\end{pmatrix};\quad H(\mu_n,\mu_l)=\begin{cases}v_n(\mu_n) & \text{in } \Omega_n^+\\ v_l(\mu_l) & \text{in } \Omega_l\setminus\Omega_b\end{cases}$$

Error splitting

$$\begin{aligned}\left\|\hat{u}_n-u^*\right\|_{0,\Omega^+} &= \left\|\hat{u}_n-L(T(\hat{u}_n))\right\|_{0,\Omega^+}+\left\|L(T(\hat{u}_n))-u^*\right\|_{0,\Omega^+}=\\ &\le \left\|\hat{u}_n-L\left(T(\hat{u}_n)\right)\right\|_{0,\Omega^+}+\left\|H\left(T(\hat{u}_n)\right)-H\left(\theta_n^*,\theta_l^*\right)\right\|_{0,\Omega^+}\\ &\le \left\|\hat{u}_n-L\left(T(\hat{u}_n)\right)\right\|_{0,\Omega^+}+\left\|H\right\|_*\left\|T(\hat{u}_n)-(\theta_n^*,\theta_l^*)\right\|_{0,\Omega^+}\end{aligned}$$

The error components

$$\left\|\hat{u}_n-L(T(\hat{u}_n))\right\|_{0,\Omega^+}$$

Consistency error

$$\left\|T(\hat{u}_n)-(\theta_n^*,\theta_l^*)\right\|_{0,\Omega^+}$$

Approximation error

$$\left\|H\right\|_*=\sup_{\{\mu_n,\mu_l\}}\frac{\left\|H(\mu_n,\mu_l)\right\|_{0,\Omega^+}}{\left\|\{\mu_n,\mu_l\}\right\|_*}$$

Lifting operator norm

Consistency error

Lemma 1

Consistency error is bounded by the modeling error on the "pure" local region:

$$\left\|\hat{u}_n - L(T(\hat{u}_n))\right\|_{0,\Omega+} = \left\|\hat{u}_n - \hat{u}_l\right\|_{0,\Omega_l \setminus \Omega_b}$$ where $\hat{u}_n$ - global nonlocal and $$\begin{cases} -\Delta \hat{u}_l = f & \text{in } \Omega_l \\ \hat{u}_l = T_l(\hat{u}_n) & \text{on } \Gamma_c \\ \hat{u}_l = 0 & \text{on } \Gamma_i \end{cases}$$

Proof. Note that $L\left(T_n(\hat{u}_n), T_l(\hat{u}_n)\right)\Big|_{\Omega_n^+} = u_n^0 + H\left(T_n(\hat{u}_n), T_l(\hat{u}_n)\right)\Big|_{\Omega_n^+} = \hat{u}_n\big|_{\Omega_n^+}$ and so,

$$L(T(\hat{u}_n)) = \begin{cases} \hat{u}_n & \text{in } \Omega_n^+ \\ \hat{u}_l & \text{in } \Omega_l \setminus \Omega_b \end{cases}$$

← Recovers the exact nonlocal solution in Ω_n^+.

← Local lifting of the exact nonlocal trace.

$$\begin{aligned} \left\|\hat{u}_n - L(T(\hat{u}_n))\right\|_{0,\Omega^+} &= \left\|\chi(\Omega_n^+)(\hat{u}_n - \hat{u}_n) + \chi(\Omega_l \setminus \Omega_b)(\hat{u}_n - \hat{u}_l)\right\|_{0,\Omega^+} \\ &= \left\|\chi(\Omega_l \setminus \Omega_b)(\hat{u}_n - \hat{u}_l)\right\|_{0,\Omega^+} \\ &= \left\|(\hat{u}_n - \hat{u}_l)\right\|_{0,\Omega_l \setminus \Omega_b} \end{aligned}$$

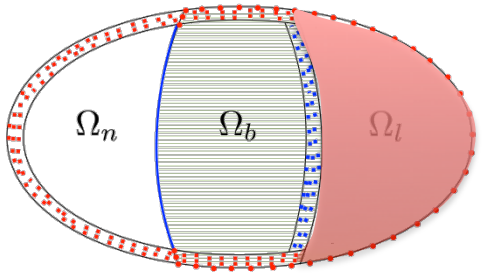

Approximation error

Sandia National Laboratories

Lemma 2

Approximation error is bounded by the modeling error on the overlap region:

$$\left\| T(\hat{u}_n) - (\theta_n^*, \theta_l^*) \right\|_* \leq \left\| \hat{u}_n - \hat{u}_l \right\|_{0,\Omega_b}$$

Proof. Using that $\left\{\theta_n^*, \theta_l^*\right\}$ solves the Euler-Lagrange equation of the reduced problem

$$\left\| T(\hat{u}_n) - \left\{\theta_n^*, \theta_l^*\right\} \right\|_* = \sup_{\{\mu_n, \mu_l\}} \frac{\left\langle T(\hat{u}_n), \left\{\mu_n, \mu_l\right\} \right\rangle_* + \left(u_n^0 - u_l^0, v_n(\mu_n) - v_l(\mu_l) \right)_{0,\Omega_b}}{\left\| \left\{\mu_n, \mu_l\right\} \right\|_*}$$

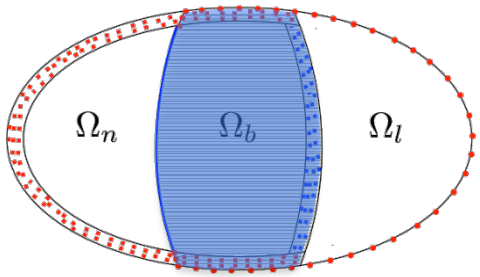

Using definition of the dual inner product

$$\begin{aligned}
&\left\langle T(\hat{u}_n), \left\{\mu_n, \mu_l\right\} \right\rangle_* + \left(u_n^0 - u_l^0, v_n(\mu_n) - v_l(\mu_l) \right)_{0,\Omega_b} \\
&\quad = \left(\hat{u}_n - \hat{u}_l, v_n(\mu_n) - v_l(\mu_l) \right)_{0,\Omega_b} \\
&\quad \leq \left\| \hat{u}_n - \hat{u}_l \right\|_{0,\Omega_b} \left\| v_n(\mu_n) - v_l(\mu_l) \right\|_{0,\Omega_b} = \left\| \hat{u}_n - \hat{u}_l \right\|_{0,\Omega_b} \left\| \left\{\mu_n, \mu_l\right\} \right\|_*
\end{aligned}$$

H is bounded from above

Sandia National Laboratories

Lemma 3

The harmonic lifting operator is bounded by a constant depending only on $|\Omega_b|$:

$$\|H\|_* = \sup_{\{\mu_n,\mu_l\}} \frac{\|H(\mu_n,\mu_l)\|_{0,\Omega^+}}{\|\{\mu_n,\mu_l\}\|_*} \le C(\Omega_b)$$

Proof. The statement is equivalent to the inequality

$$\|v_n(\mu_n)\|^2_{0,\Omega_n^+} + \|v_l(\mu_l)\|^2_{0,\Omega_l\setminus\Omega_b} \le C^2(\Omega_b)\,\|v_n(\mu_n) - v_l(\mu_l)\|^2_{0,\Omega_b} \quad \forall \{\mu_n,\mu_l\} \in \Lambda_n \times \Lambda_l$$

Furthermore:

$$\|\mu_n\|_{\tilde{V}(\tilde{\Omega}_n^+)} \le c_n \|v_n(\mu_n)\|_{E,\Omega_b} \le K_n \|v_n(\mu_n)\|_{0,\Omega_b} \quad \rightarrow \quad \|v_n(\mu_n)\|^2_{0,\Omega_n^+} \le K_n \|v_n(\mu_n)\|^2_{0,\Omega_b}$$

Trace ↕ Caccioppoli ↕

$$\|\mu_l\|_{\frac{1}{2},\Gamma_c} \le c_l \|v_l(\mu_l)\|_{1,\Omega_b} \le K_l \|v_l(\mu_l)\|_{0,\Omega_b} \quad \rightarrow \quad \|v_l(\mu_l)\|^2_{0,\Omega_l\setminus\Omega_b} \le K_l \|v_l(\mu_l)\|^2_{0,\Omega_b}$$

H is bounded from above

Sandia National Laboratories

Proof of nonlocal trace and Caccioppoli inequalities requires the kernel assumption

$$\overline{\gamma}_k < \infty \quad where \quad \overline{\gamma}_k = \left\| \gamma_k \right\|_{\infty,\Omega}^{1/k}, \quad \gamma_k = \int_{\Omega} \gamma^k(x,y)\, dy$$

Now the statement of the theorem boils down to

$$\left\| v_n(\mu_n) \right\|_{0,\Omega_b}^2 + \left\| v_l(\mu_l) \right\|_{0,\Omega_b}^2 \le C^2(\Omega_b) \left\| v_n(\mu_n) - v_l(\mu_l) \right\|_{0,\Omega_b}^2 \qquad \forall \left\{ \mu_n, \mu_l \right\} \in \Lambda_n \times \Lambda_l$$

Which follows from the strong Cauchy-Schwartz inequality

$$\left| \left(v_n(\mu_n), v_l(\mu_l) \right)_{0,\Omega_b} \right| \le (1-\delta) \left\| v_n(\mu_n) \right\|_{0,\Omega_b} \left\| v_l(\mu_l) \right\|_{0,\Omega_b}; \qquad 0 < \delta < 1$$

The proof of strong CBS again requires the kernel assumptions.

Modeling error

Recall our main result

Theorem

LtN **coupling error** is bounded by the **modeling error** on the **local subdomain**:

$$\left\| \hat{u}_n - u^* \right\|_{0,\Omega^+} \leq (1 + C(\Omega_b)) \left\| \hat{u}_n - \hat{u}_l \right\|_{0,\Omega_l}$$

We make the assumption that the restriction of the nonlocal solution to the local region is of class C^4

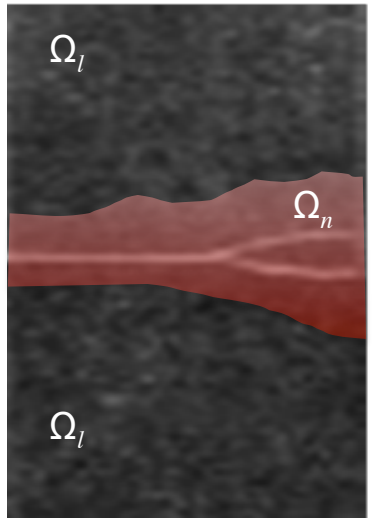

Corollary

Modeling error is bounded by the square of the interaction radius

$$\left\| \hat{u}_n - \hat{u}_l \right\|_{0,\Omega_l} \leq C\varepsilon^2 + O(\varepsilon^4)$$

Numerical examples

Problem setting in 1D

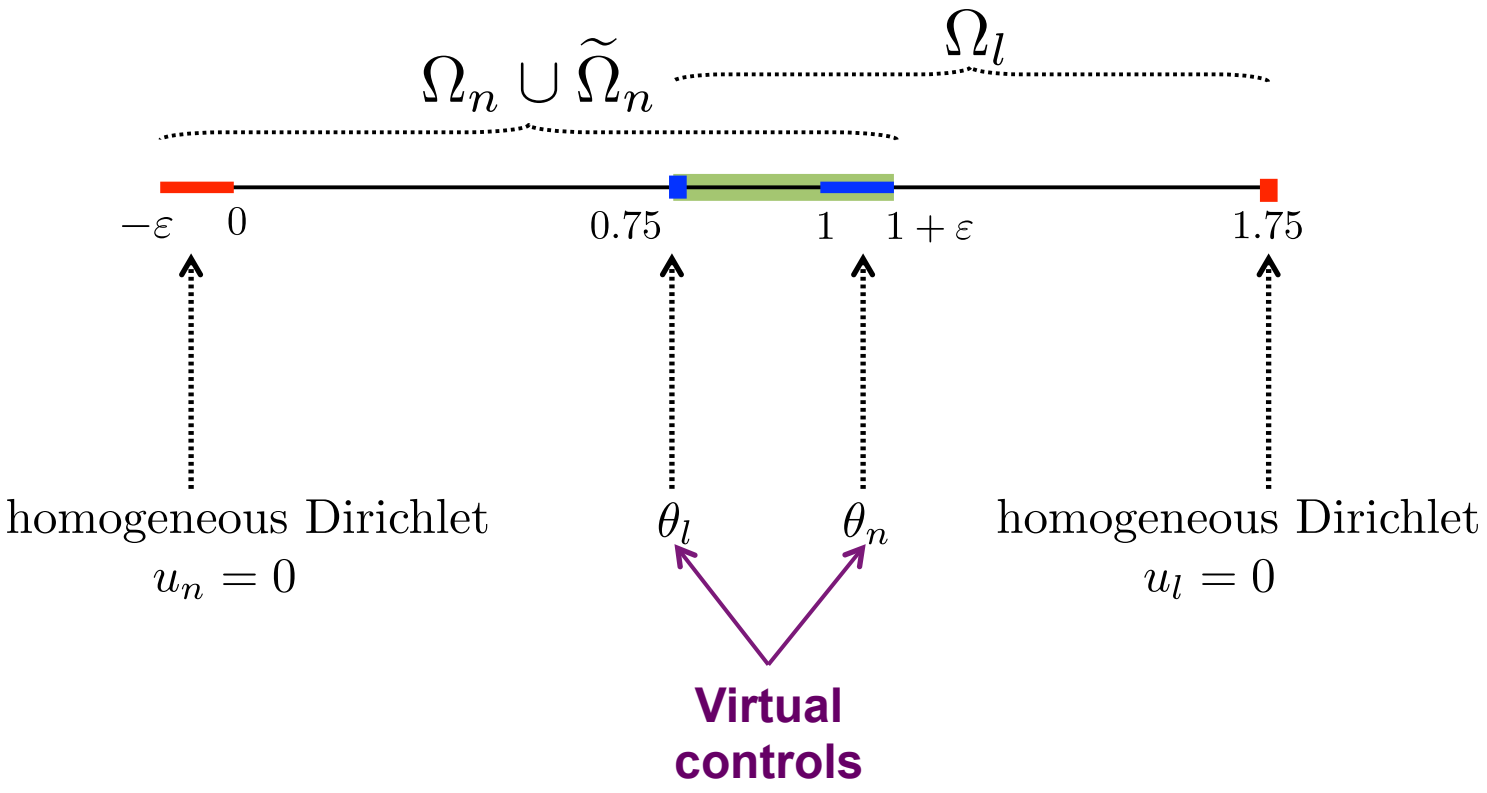

Patch test

Kernel: $\gamma(x,y) = \dfrac{1}{\varepsilon^2|x-y|}\chi(x-\varepsilon, x+\varepsilon)$

Exact solution:

- $u_n = u_l = x$
- $u_n|_{\widetilde{\Omega}_i} = x$
- $u_l(1.75) = 1.75$
- $f_n = f_l = 0$

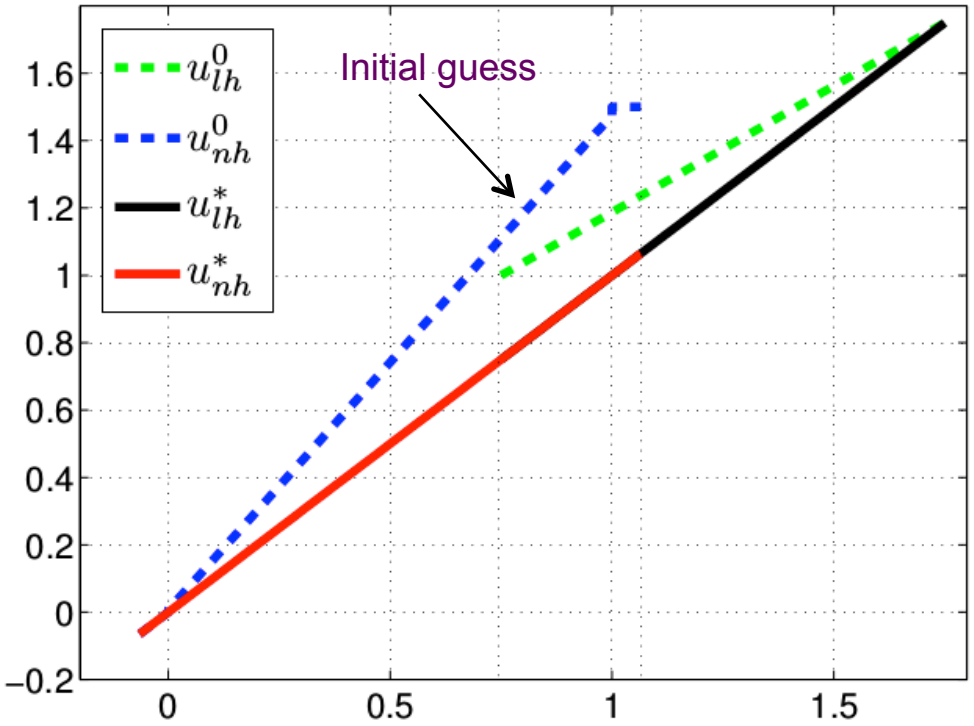

Smooth global solution

Sandia National Laboratories

Example 1

- $u_n = u_l = x^2$
- $u_n|_{\widetilde{\Omega}_i} = x^2$
- $u_l(1.75) = 1.75^2$
- $f_n = f_l = -2$

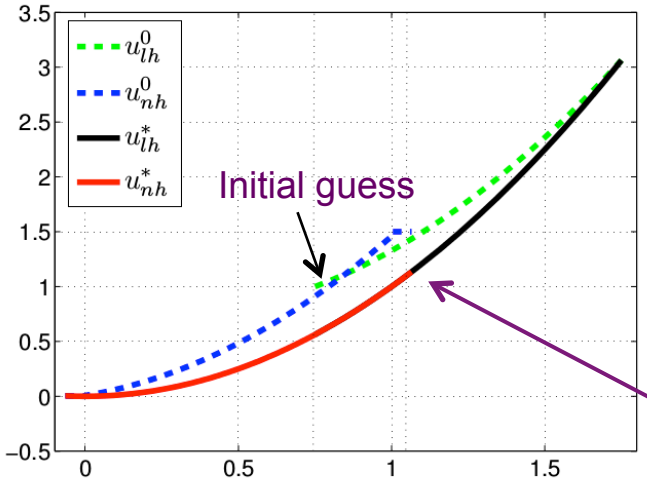

ε	h	$e(u_n)$	rate	$e(u_l)$	rate
0.065 test 1.	2^{-3}	2.36e-03	-	2.62e-03	-
	2^{-4}	7.54e-04	1.65	7.12e-04	1.88
	2^{-5}	1.88e-04	2.00	1.78e-04	2.00
	2^{-6}	4.67e-05	2.01	4.44e-05	2.00
	2^{-7}	1.14e-05	2.04	1.10e-05	2.01

Optimization approach merges the models seamlessly!

Example 2

- $u_n = u_l = x^2 - x^4$
- $u_n|_{\widetilde{\Omega}_i} = x^2 - x^4$
- $u_l(1.75) = 1.75^2 - 1.$
- $f_n = -2 + 12x^2 + \varepsilon^2$
- $f_l = -2 + 12x^2.$

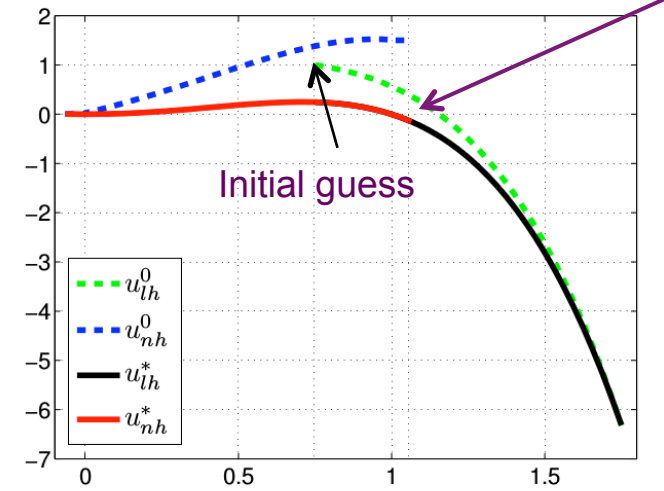

ε	h	$e(u_n)$	rate	$e(u_l)$	rate
0.065 test 2.	2^{-3}	9.70e-03	-	2.95e-02	-
	2^{-4}	2.68e-03	1.86	7.54e-03	1.97
	2^{-5}	7.02e-04	1.93	1.90e-03	1.99
	2^{-6}	1.78e-04	1.98	4.76e-04	2.00
	2^{-7}	4.48e-05	1.99	1.19e-04	2.00

Rough nonlocal solution

Demonstrate the effectiveness of the coupling method in the presence of "real" nonlocal effects

Point force

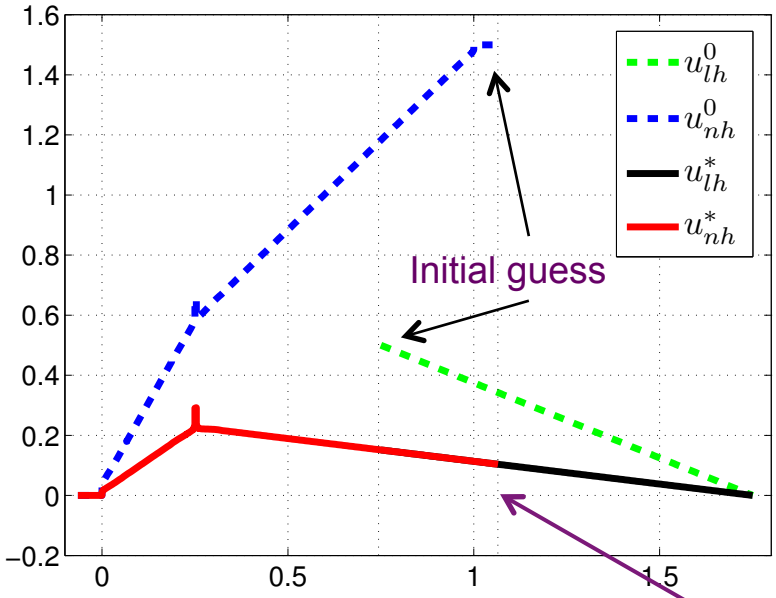

Discontinuous nonlocal state

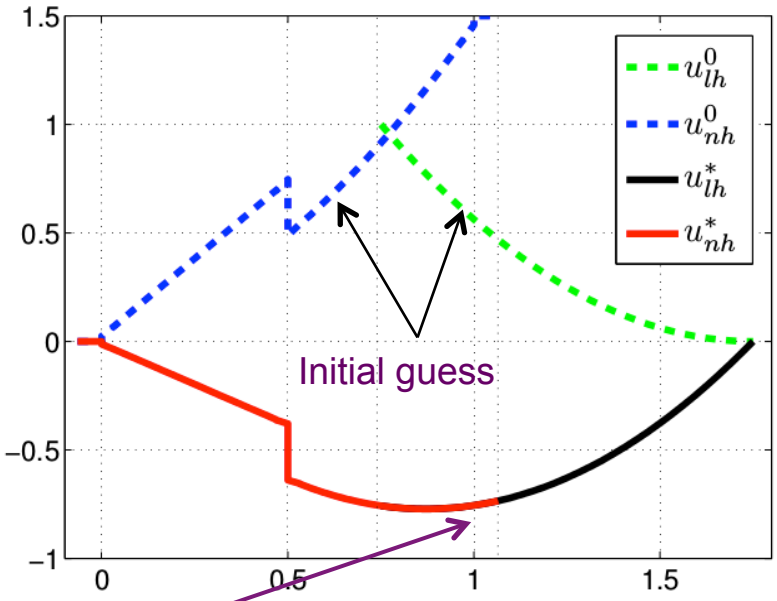

Optimization approach merges the models seamlessly!

Absence of ghost forces

Sandia National Laboratories

Point force

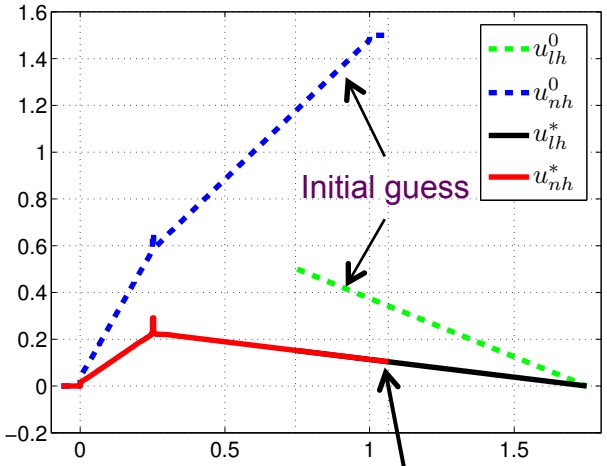

Discontinuous nonlocal

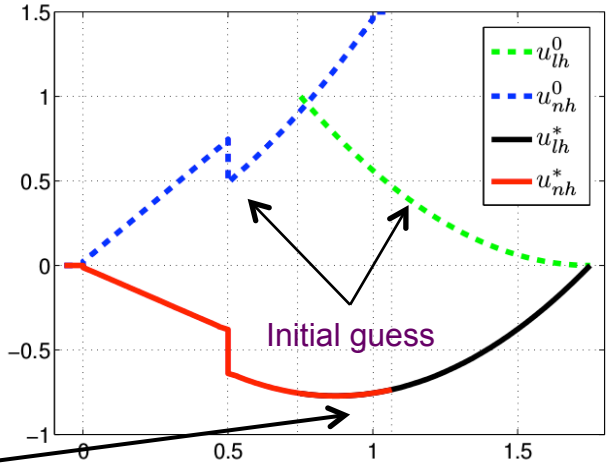

Optimization coupling eliminates ghost forces because it does not try to enforce equality of disparate states, rather it tries to minimize their mismatch.

On the contrary, ghost forces are very difficult to avoid in formulations where coupling conditions are hard constraints enforcing equality of disparate states.

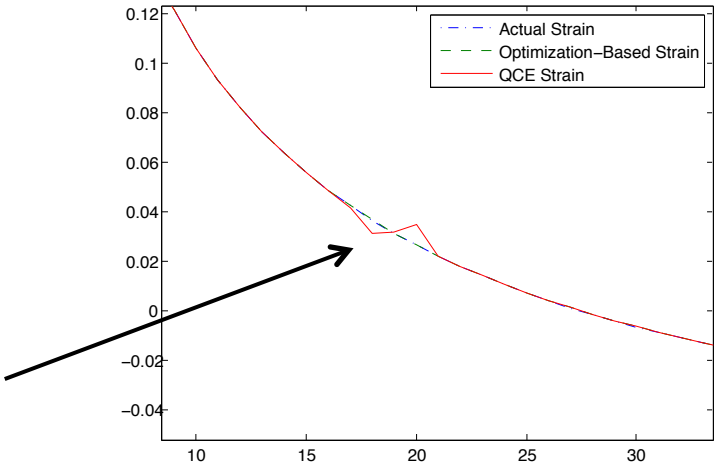

Ghost force example; Luskin et al.

Crossing the valley of death

Sandia National Laboratories

Research & proof-of-principle →  → **Programmatically exercised software**

Significance of the agile components approach:

- Provide access to adjoints, sensitivites, etc. for adjoint-based fast optimization.
- Enable effective transitioning of research ideas into powerful production software.

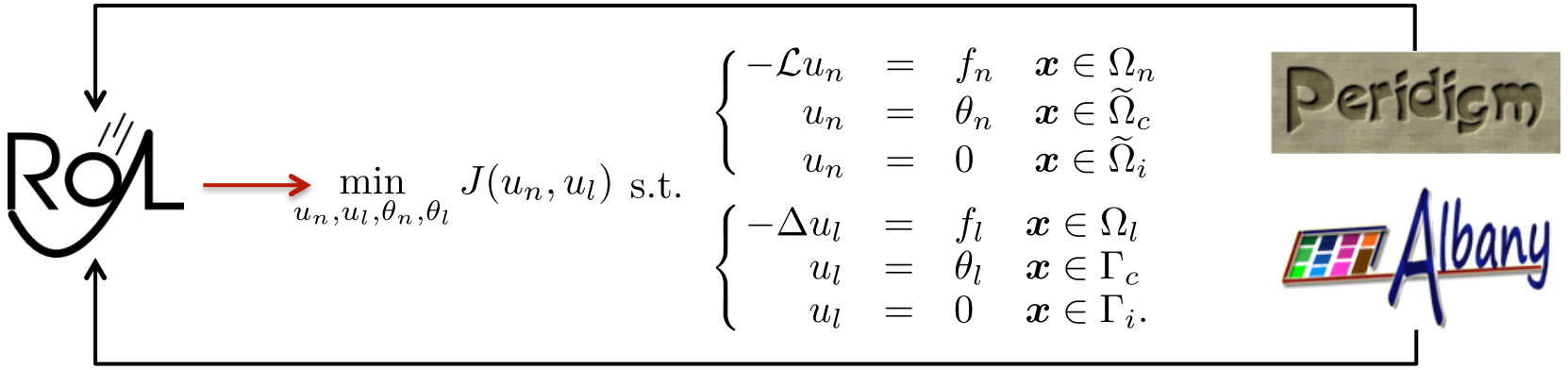

Collaboration with D. Littlewood, M. D'Elia, M. Perego

- Provides a new material simulation capability with unique mathematical and computational properties that are not currently available by other means.
- Can be used as a "**corrector**" to a conventional coupling to improve its accuracy.

LtN coupling of Peridigm+Albany

Sandia National Laboratories

Linear consistency test

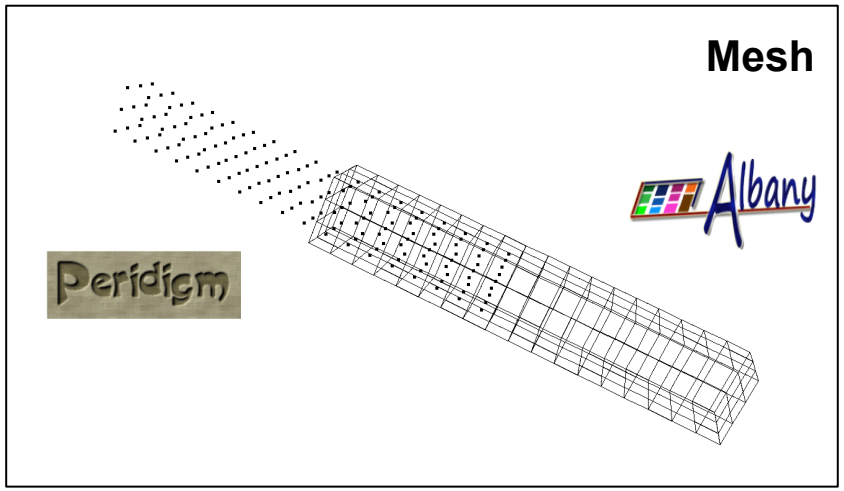

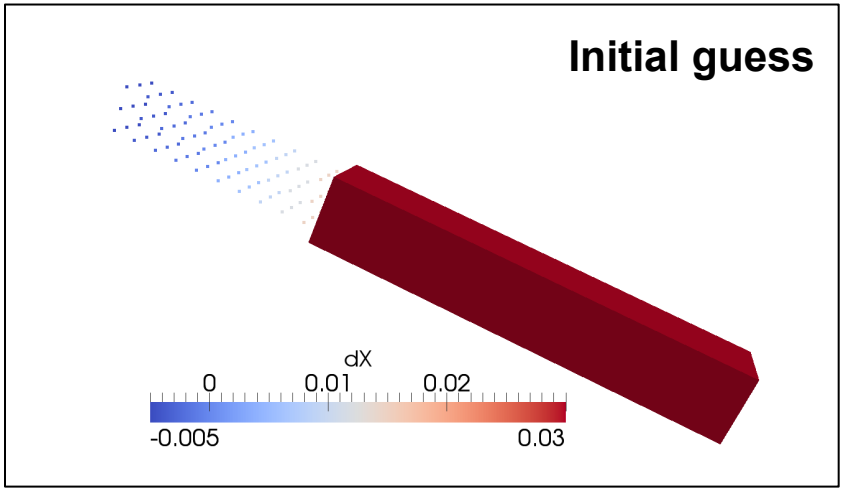

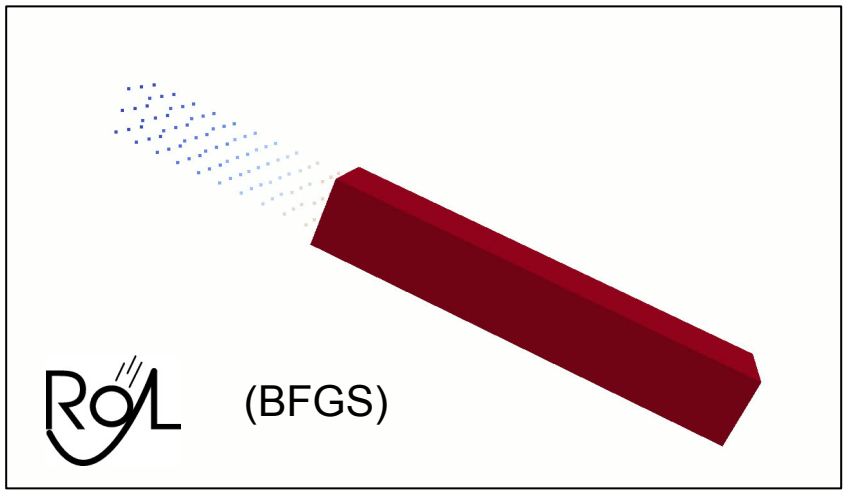

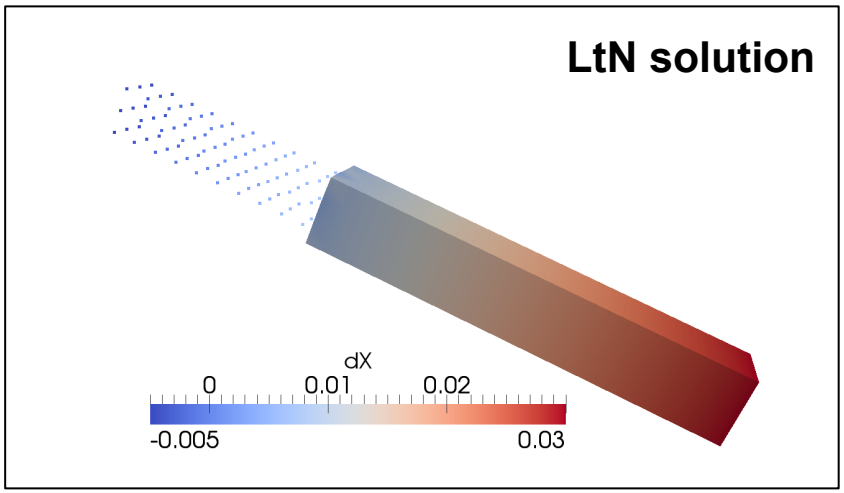

References

1. D. Olson, M. Luskin, A. Shapeev and P. Bochev, Analysis of an optimization-based atomistic-to-continuum coupling method for point defects. To appear in *ESAIM (Mathematical Modeling and Numerical Analysis)*. SAND2014-18401J.
2. D. Olson, P. Bochev, M. Luskin and A. Shapeev. An optimization-based atomistic-to-continuum coupling method. *SIAM. J. Num. Anal*.. Vol. 52, Issue 4, pp.2183-2204 (2014)
3. D. Olson, P. Bochev, M. Luskin and A. Shapeev. Development of an optimization-based atomistic-to-continuum coupling method. In. Lirkov, Wasniewski, editors, Large-Scale Scientific Computing, Vol. 8353, LNCS, pp. 33-44, Springer Berlin, Heidelberg, 2014.
4. M. D'Elia and P. B. Bochev. Optimization-based local-to-nonlocal coupling method, Sandia Technical Report, No. SAND2014-17373J (2014).
5. M. D'Elia and P. B. Bochev, Optimization-Based Coupling of Nonlocal and Local Diffusion Models. *Materials Research Society Proceeding*, (2014) .
6. M. D'Elia and P. Bochev, Formulation, analysis and computation of an optimization-based local-to-nonlocal coupling method. Submitted to *SIAM. J. Num. Anal*. SAND2014-17373J.

Sandia National Laboratories

Part 2

Case study 2: Transport schemes

In Part 2 we apply optimization ideas to develop property-preserving methods for transport of passive tracers in climate models.

Minimize

Coupling mismatch $\left\|u_1^h - u_2^h\right\|^2$ + $\sum_i \left\|u_i^h - u_i^T\right\|^2$ **Target mismatch**

Subject to

Target definition $L_1^h(u_1^T, \theta) = f_1$ $\quad \underline{C}_i \le C u_i^h \le \overline{C}_i$ **Physical properties**

$L_2^h(u_2^T, \theta) = f_2$ $\quad B u_i^h = b$

This case study highlights application of optimization ideas for the preservation of relevant physical properties in numerical methods.

P. Bochev, D. Ridzal, M. Shashkov, Fast optimization-based conservative remap of scalar fields, J. Comp. Phys. 246 (2013)

P. Bochev, D. Ridzal, K. Peterson, Optimization-based remap and transport: A divide and conquer strategy for feature- preserving discretizations, J. Comp. Phys. 257, (2014) 1113 – 1139.

Transport of passive tracers

Sandia National Laboratories

Governing equations

$$\left.\begin{aligned} &\frac{\partial \rho}{\partial t} + \nabla \cdot \rho \mathbf{u} = 0 \\ &\frac{\partial \rho q}{\partial t} + \nabla \cdot \rho q \mathbf{u} = 0 \end{aligned}\right\} \Rightarrow \quad \frac{\partial q}{\partial t} + \mathbf{u} \cdot \nabla q = 0$$

where:

- ρ - density
- q - tracer mixing ratio
- $\mathbf{u}$ - velocity

Key requirements

1. Conservation of mass and total tracer: $M = \int_\Omega \rho \, dV \qquad Q = \int_\Omega \rho q \, dV$
2. Preservation of local bounds for q and ρ: $\rho_i^{\min} \le \rho_i \le \rho_i^{\max} \qquad q_i^{\min} \le q_i \le q_i^{\max}$
3. Preservation of linear correlations between tracers: $q_1(x) = a q_2(x) + b$
4. Preservation of constant tracers, i.e., "compatibility"

We begin Part 2 by developing a new scheme, which combines

- Spectral elements (SE) for spatial discretization.
- Semi-Lagrangian (SL) approach for time stepping.
- Optimization for enforcing conservation and local bounds.

Why SE + SL?

Sandia National Laboratories

Advantages

- **Diagonal** mass matrix
- **Spectral** accuracy
- **Avoids severe CFL** restrictions of high-order methods
- **Simple!!** (compare, e.g., to tent-pitching schemes)
- **HOMME** (High Order Modeling Environment) uses SE and DG on fully unstructured quadrilateral meshes on the sphere such as the cubed-sphere mesh.

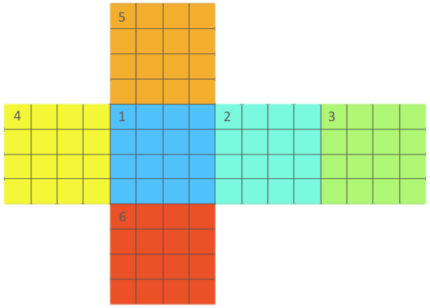

cubed-sphere mesh

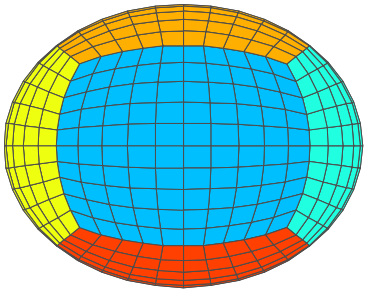

HOMME is a community model supported by the NSF and the DOE with contributions from NCAR, DOE laboratories and universities.

HOMME is the default dynamical core of the Community Atmosphere Model (CAM) and the Community Earth System Model (CESM)

The new SL-SE scheme for tracers is motivated by and implemented in HOMME.

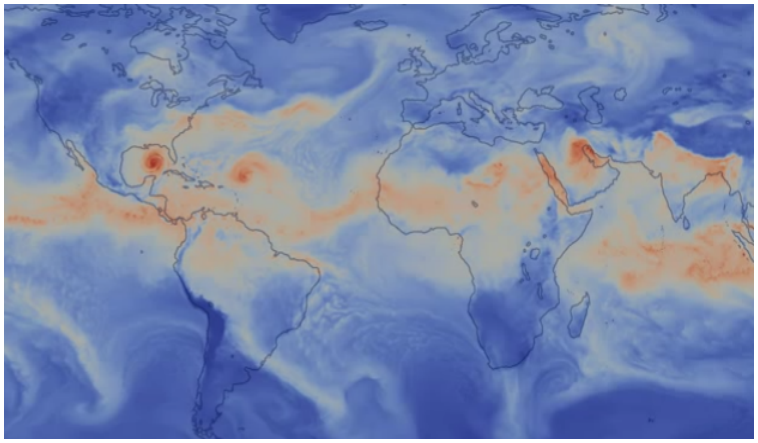

Dennis J, Edwards J, Evans K, Guba O, Lauritzen P, Mirin A, St.-Cyr A, Taylor M, Worley P. 2012. CAM-SE: A scalable spectral element dynamical core for the Community Atmosphere Model. IJHPCA. 26:74-89.

A generic SL transport scheme

Key idea: convert PDEs into ODEs along Lagrangian particle paths

$$\left\{\begin{array}{l} \dfrac{\partial \rho}{\partial t} + \nabla \cdot \rho \mathbf{u} = 0 \rightarrow \dfrac{\partial \rho}{\partial t} + \mathbf{u} \cdot \nabla \rho = -\rho \nabla \cdot \mathbf{u} \\ \dfrac{\partial \rho q}{\partial t} + \nabla \cdot \rho q \mathbf{u} = 0 \rightarrow \dfrac{\partial q}{\partial t} + \mathbf{u} \cdot \nabla q = 0 \end{array}\right\} \rightarrow \frac{dx}{dt} = \mathbf{u}(x(t),t) \rightarrow \left\{\begin{array}{l} \dfrac{D\rho}{Dt} = -\rho \nabla \cdot \mathbf{u} \\ \dfrac{Dq}{Dt} = 0 \end{array}\right.$$

Step 1: solve the "final value" problem in $[t_n, t_{n+1}]$:

$$\frac{dx}{dt} = \mathbf{u}(x(t),t) \text{ and } x(t_{n+1}) = \mathbf{p} \rightarrow \tilde{\mathbf{p}} = x(t_n)$$

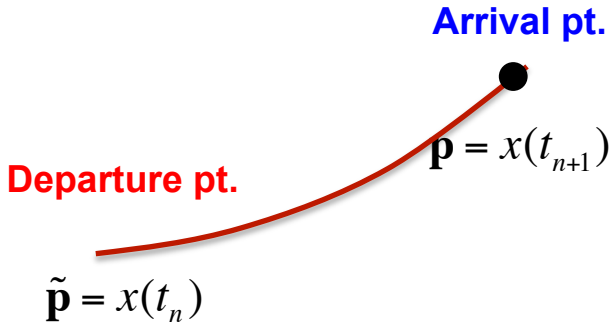

Step 2: solve the initial value problems in $[t_n, t_{n+1}]$:

$$\frac{D\rho}{Dt} = -\rho \nabla \cdot \mathbf{u} \text{ and } \rho(t_n) = \rho_h(\tilde{\mathbf{p}}, t_n) \rightarrow \rho_h(\mathbf{p}, t_{n+1}) = \rho(t_{n+1})$$

ODE solution at t_{n+1} = PDE solution at **arrival pt.**

$$\frac{Dq}{Dt} = 0 \text{ and } q(t_n) = q_h(\tilde{\mathbf{p}}, t_n) \rightarrow q_h(\mathbf{p}, t_{n+1}) = q(t_{n+1})$$

Initial value at t_n = PDE solution at **departure pt.**

Combine with SE reconstruction

Step 1: solve the "final value" problem in $[t_n, t_{n+1}]$:

$$\frac{dx}{dt} = \mathbf{u}(x(t),t) \quad \text{and} \quad x(t_{n+1}) = \mathbf{p}_{ij}$$

$\{\mathbf{p}_{ij}\}$ → Arrival points = Gauss-Lobatto points

$\{\tilde{\mathbf{p}}_{ij}\}$ → Departure points

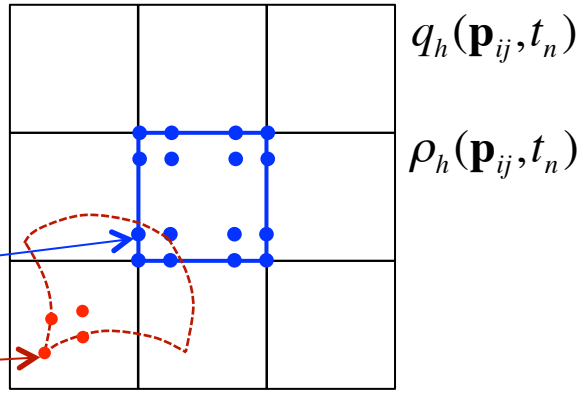

Step 2: solve the initial value problems in $[t_n, t_{n+1}]$:

$$\frac{D\rho}{Dt} = -\rho \nabla \cdot \mathbf{u} \quad \text{and} \quad \rho(t_n) = \rho_h(\tilde{\mathbf{p}}_{ij}, t_n)$$

$$\frac{Dq}{Dt} = 0 \qquad \text{and} \quad q(t_n) = q_h(\tilde{\mathbf{p}}_{ij}, t_n)$$

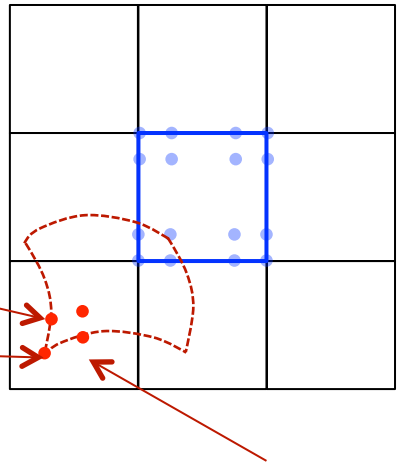

Initial values = spectral element reconstruction at Gauss-Lobatto **departure points**

Example: rotation

$$\frac{dx}{dt} = \mathbf{u}(x(t),t) \quad \text{and} \quad x(t_{n+1}) = \mathbf{p}_{ij}$$

$$\mathbf{u}(x(t),t) = \begin{pmatrix} 0.5 - y \\ 0.5 - x \end{pmatrix}$$

Solved by RK4

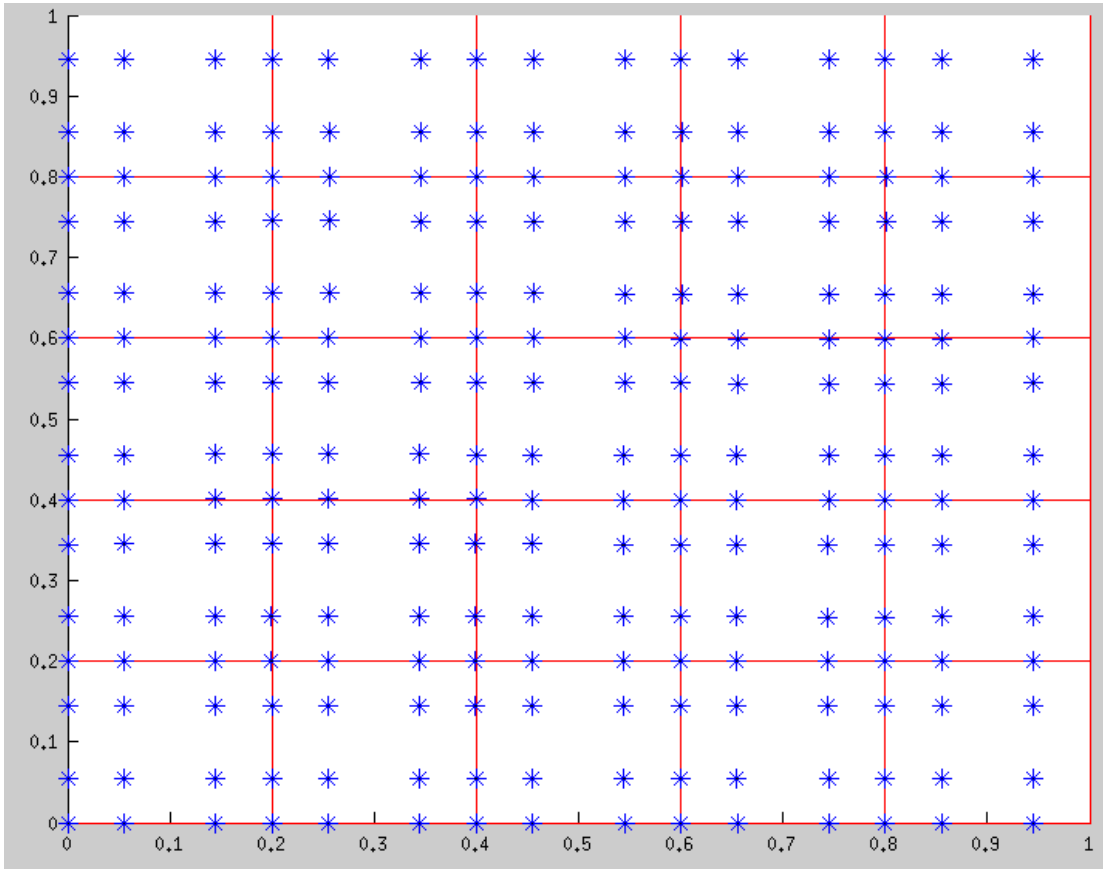

Generic SE+SL scheme scorecard

Sandia National Laboratories

Recall the advantages:

- **Diagonal** mass matrix
- **Spectral** accuracy
- **Avoids severe CFL** restrictions of high-order methods
- **Simple!!** (compare, e.g., to tent-pitching schemes)

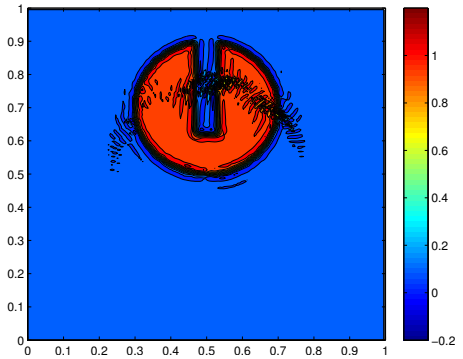

However, the generic scheme

- **Does not conserve mass and total tracer**
- **Does not preserve local solution bounds**

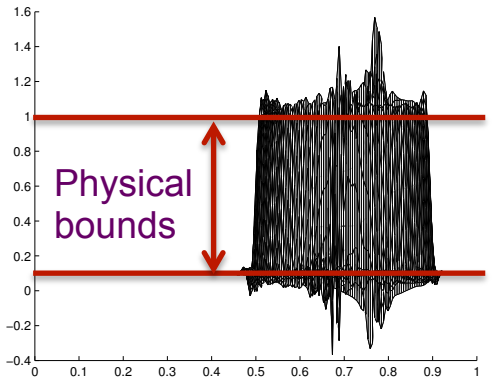

Critical for physically consistent tracer transport, since high-order spatial schemes are prone to unphysical oscillations:

Solution: combine the generic SE+SL scheme with optimization to

- **Conserve mass and total tracer**
- **Preserve local solution bounds**

Optimization-based SE-SL scheme

Sandia National Laboratories

Start with a generic SE+SL scheme:

1. Determine GL departure points → $\tilde{\mathbf{p}}_{ij} = x(t_n)$
2. Determine solution at arrival points → $\rho_h(\mathbf{p}_{ij}, t_{n+1}) = \rho(t_{n+1})$ and $q_h(\mathbf{p}_{ij}, t_{n+1}) = q(t_{n+1})$

Then proceed as follows to find the tracer at t_{n+1} (density is similar)

3. Set optimization target to SE+SL solution: $\hat{q} := q_h(\mathbf{p}_{ij}, t_{n+1})$
4. Determine local solution bounds: $q_{ij}^{\min} \le q(\mathbf{p}_{ij}, t_{n+1}) \le q_{ij}^{\max}$ → **TBD later!**
5. Set solution at the new time step by solving

$$q_{n+1}^{*} = \underset{q \in Q^r}{\operatorname{argmin}} \left\| q - \hat{q} \right\|_0^2 \quad \text{subject to} \quad \begin{cases} \int_\Omega q\,dx = \int_\Omega q_n\,dx & \leftarrow \text{Conservation} \\ q_{ij}^{\min} \le q_{ij} \le q_{ij}^{\max} & \leftarrow \text{Local bounds} \end{cases}$$

The optimization problem

Sandia National Laboratories

Algebraic form

$$\mathbf{q}_{n+1} = \underset{\mathbf{q}}{\operatorname{argmin}}\, \mathbf{q}^T\mathbf{M}\mathbf{q} + \mathbf{c}^T\mathbf{q} + \mathbf{c}_0 \quad \text{subject to} \quad \begin{cases} \mathbf{w}^T\mathbf{q} = \mathbf{w}^T\mathbf{q}_n & \leftarrow \text{Conservation} \\ \mathbf{q}^{\min} \le \mathbf{q} \le \mathbf{q}^{\max} & \leftarrow \text{Local bounds} \end{cases}$$

$$\mathbf{M} = \int_{\Omega} \phi_{ij}\phi_{kl}\, dx = diag(M_{ij}); \quad \mathbf{c} = -2\mathbf{M}\hat{\mathbf{q}}; \quad \mathbf{c}_0 = \hat{\mathbf{q}}^T\mathbf{M}\hat{\mathbf{q}}; \quad \mathbf{w} \rightarrow \text{Gauss-Lobato weights}$$

- ☞ Example of a "*singly linearly constrained QP with simple bounds*"
- ☞ QP structure admits a fast *O(N)* optimization algorithm.

Theorem (Existence of optimal solutions)

The feasible set of the optimization problem for the solution transfer is non-empty. The problem has a unique optimal solution.

Fast Optimization Algorithm

Sandia National Laboratories

Without the equality constraint the QP splits into *N* one-dimensional QPs with simple bounds:

$$q_{ij,n+1} = \underset{q_{ij}}{\operatorname{argmin}} M_{ij}\left(q_{ij} - \hat{q}_{ij}\right)^2 \quad \text{subject to} \quad q_{ij}^{\min} \le q_{ij} \le q_{ij}^{\max}$$

$$\Rightarrow \quad q_{ij,n+1} = med(q_{ij}^{\min}, \hat{q}_{ij}, q_{ij}^{\max})$$

The Lagrangian

$$L(\mathbf{q}, \lambda, \mu_1, \mu_2) = \sum_{node} M_{ij}\left(q_{ij} - \hat{q}_{ij}\right)^2 - \lambda \sum_{node} w_{ij}\left(q_{ij} - q_{ij,n}\right) - \sum_{node} \mu_{1,ij}(q_{ij} - q_{ij}^{\min}) - \sum_{node} \mu_{2,ij}(q_{ij} - q_{ij}^{\max})$$

The Karush-Kuhn-Tucker (KKT) conditions

$$\begin{cases} q_{ij} = \hat{q}_{ij} + \lambda + \mu_{1,ij} - \mu_{2,ij} \\ q_{ij}^{\min} \le q_{ij} \le q_{ij}^{\max} \\ \mu_{1,ij} \ge 0, \quad \mu_{2,ij} \ge 0 \\ \mu_{1,ij}(q_{ij} - q_{ij}^{\min}) = 0, \\ \mu_{2,ij}(q_{ij} - q_{ij}^{\max}) = 0 \end{cases} \quad \text{and} \quad \sum_{node} w_{ij}\left(q_{ij} - q_{ij,n}\right) = 0$$

Without the equality constraint the KKT conditions are fully separable and can be solved for any fixed value of λ.

Fast Optimization Algorithm

Sandia National Laboratories

Step 1: solve for λ fixed

$$\begin{cases} q_{ij} = \tilde{q}_{ij} + \lambda;\ \mu_{1,ij} = 0;\ \mu_{2,ij} = 0 & \text{if}\quad q_{ij}^{\min} \le \tilde{q}_{ij} + \lambda \le q_{ij}^{\max} \\ q_{ij} = q_{ij}^{\min};\quad \mu_{2,ij} = 0;\ \mu_{1,ij} = q_{ij} - \tilde{q}_{ij} - \lambda & \text{if}\quad q_{ij}^{\min} \ge \tilde{q}_{ij} + \lambda \\ q_{ij} = q_{ij}^{\max};\quad \mu_{1,ij} = 0;\ \mu_{2,ij} = \tilde{q}_{ij} - q_{ij} + \lambda & \text{if}\quad \tilde{q}_{ij} + \lambda \ge q_{ij}^{\max} \end{cases} \Rightarrow q_{ij}(\lambda) = med(q_{ij}^{\min}, \tilde{q}_{ij} + \lambda, q_{ij}^{\max});$$

Trivial, communication-free O(N) computation

Step 2: adjust λ in an outer iteration to satisfy the single equality constraint

$$\text{Solve} \quad \sum_{node} w_{ij}\left(q_{ij}(\lambda) - q_{ij,n}\right) = 0 \Rightarrow$$

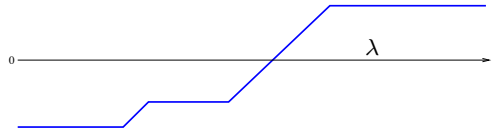

- Piecewise linear, monotonically increasing function of single scalar variable λ
- Can solve to machine precision by a simple secant method
- Globalization is unnecessary: $\lambda_0 = 0$ is an excellent initial guess: $q_{ij}(\lambda_0) = med(q_{ij}^{\min}, \tilde{q}_{ij}, q_{ij}^{\max});$
- $q_{ij}(\lambda_0)$ solves the QP without the equality constraint, i.e., "almost" a solution
- Locality $\Rightarrow q_{ij}(\lambda_0)$ barely violates the mass conservation constraint

Local solution bounds: $\nabla \cdot \mathbf{u} = 0$

For solenoidal fields Step 2 is trivial:

$$\frac{D\rho}{Dt} = 0 \quad \Rightarrow \quad \rho(x(t),t) = const \quad \rightarrow \quad \rho_h(\mathbf{p}_{ij}, t_{n+1}) = \rho(t_{n+1}) = \rho(t_n) = \rho_h(\tilde{\mathbf{p}}_{ij}, t_n)$$

$$\frac{Dq}{Dt} = 0 \quad \Rightarrow \quad q(x(t),t) = const \quad \rightarrow \quad q_h(\mathbf{p}_{ij}, t_{n+1}) = q(t_{n+1}) = q(t_n) = q_h(\tilde{\mathbf{p}}_{ij}, t_n)$$

Solution is constant along Lagrangian paths ⇒ taking min/max in a neighborhood of the departure points is sufficient to determine solution bounds:

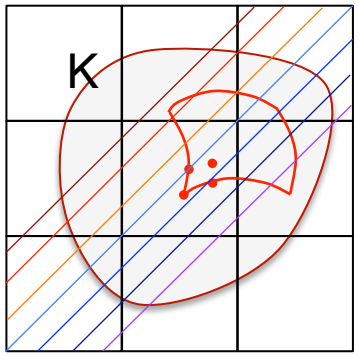

$$q_{ij}^{\min} = \min_{\mathbf{p} \in K} q(\mathbf{p}_{ij}, t_n)$$

$$q_{ij}^{\max} = \max_{\mathbf{p} \in K} q(\mathbf{p}_{ij}, t_n)$$

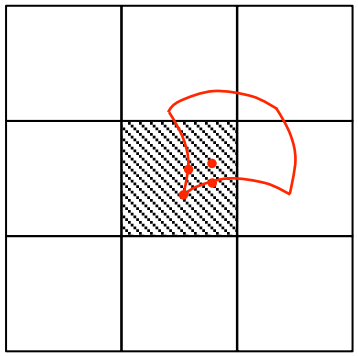

Tight bounds

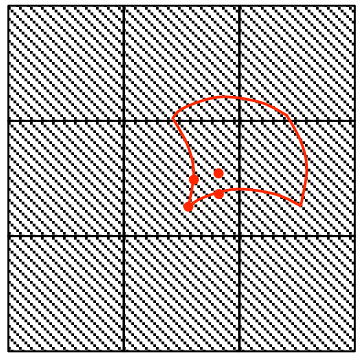

Loose bounds

Rotational flow: LeVeque's combo

Zalesak cylinder, cone and a smooth hump

$$\mathbf{u}(\mathbf{p},t) = \begin{pmatrix} 0.5 - y \\ 0.5 - x \end{pmatrix}$$

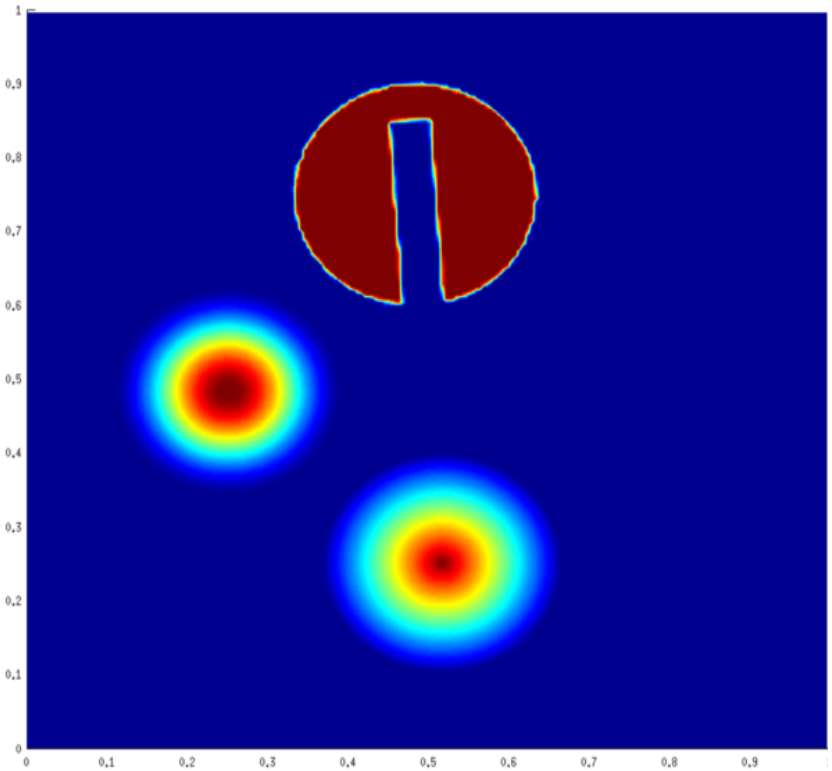

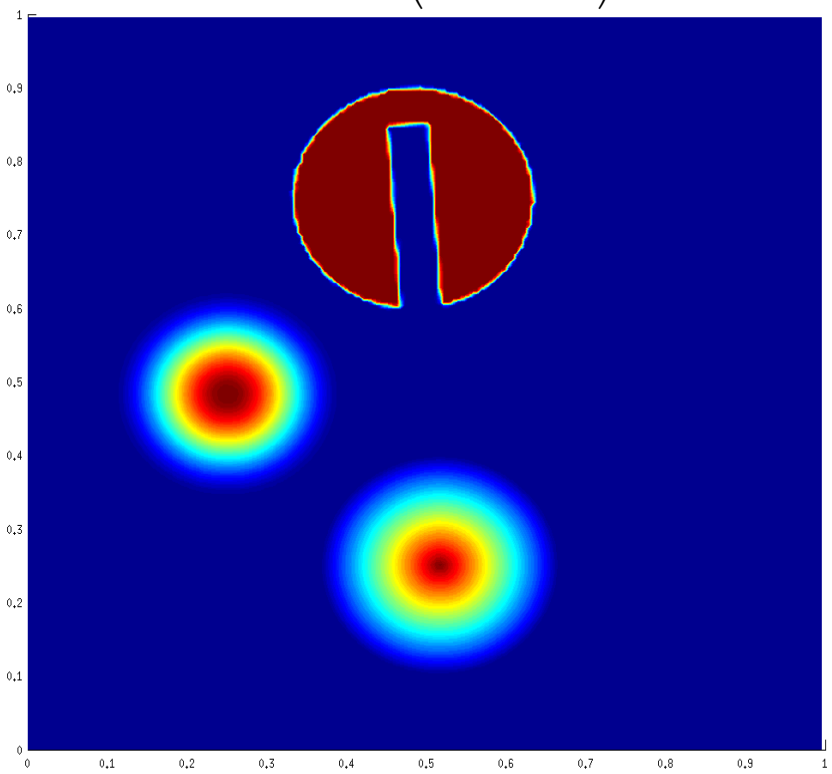

80x80 bi-cubic elements; CFL=0.7

R. J. LeVeque, High-resolution conservative algorithms for advection in incompressible flow, SINUM 33 (1996) 627–665.

Deformational flow: cosine bell

$$q(x,t) = 0.5(1.0 + \cos(\pi r_1)); \quad r_1 = \frac{\min(r, r_0)}{r_0}$$

$$\mathbf{u}(\mathbf{p},t) = \begin{pmatrix} \sin(\pi x)^2 \sin(2\pi y)\cos(\pi t / T) \\ -\sin(\pi y)^2 \sin(2\pi x)\cos(\pi t / T) \end{pmatrix}$$

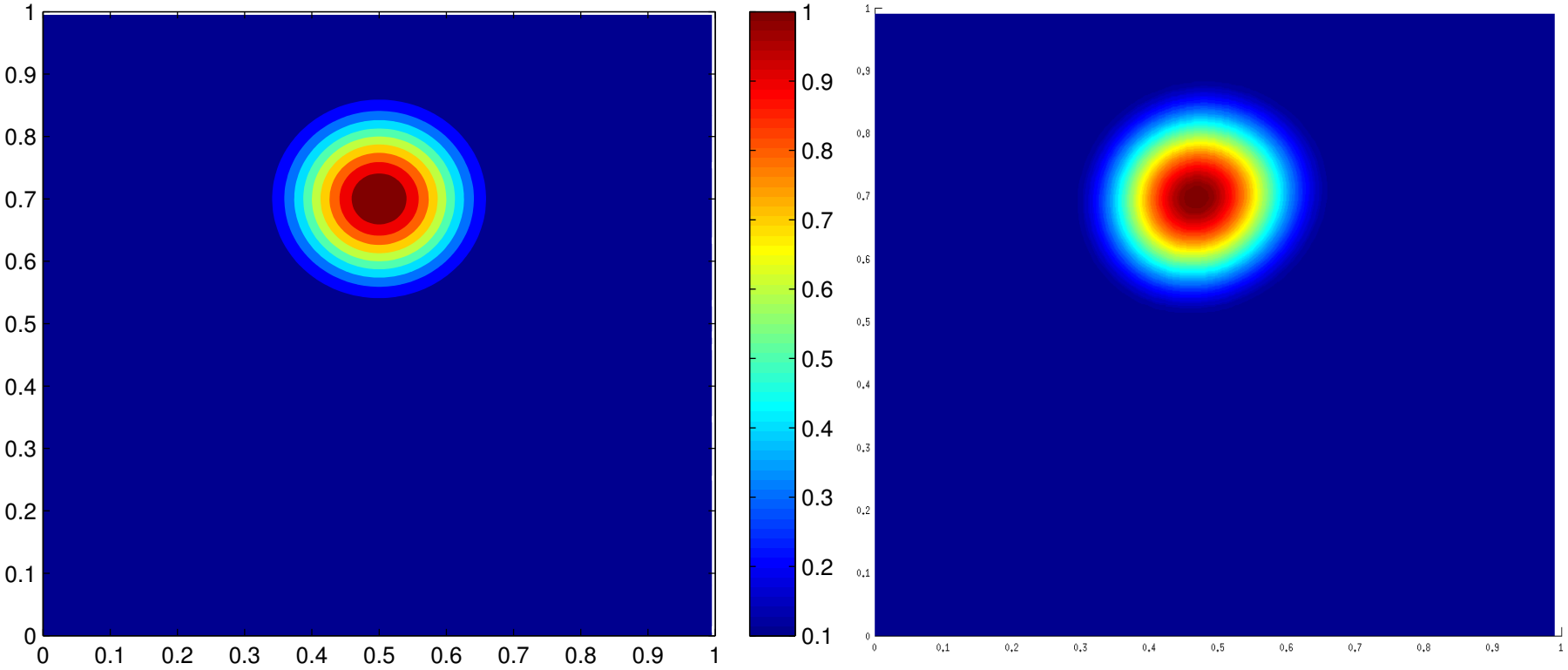

80x80 bi-cubic elements; CFL=0.7

R. J. LeVeque, High-resolution conservative algorithms for advection in incompressible flow, SINUM 33 (1996) 627–665.

Convergence rates: Gaussian hill

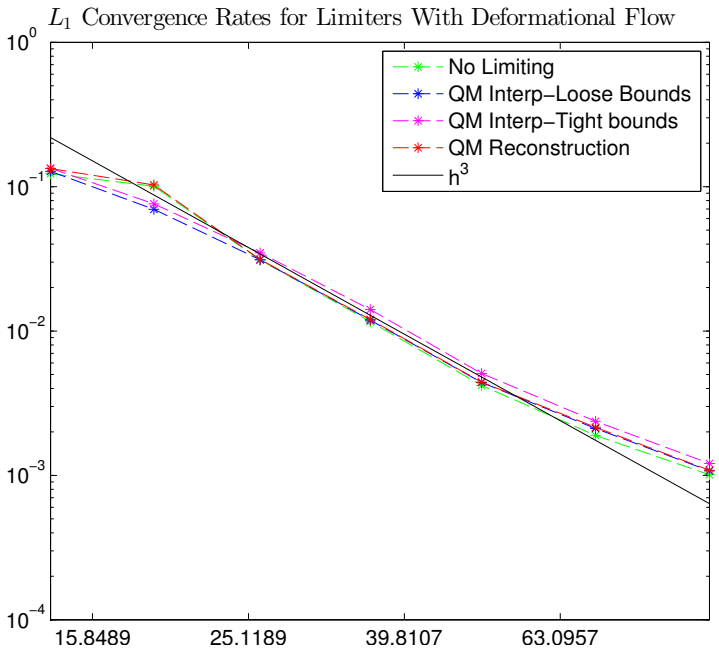

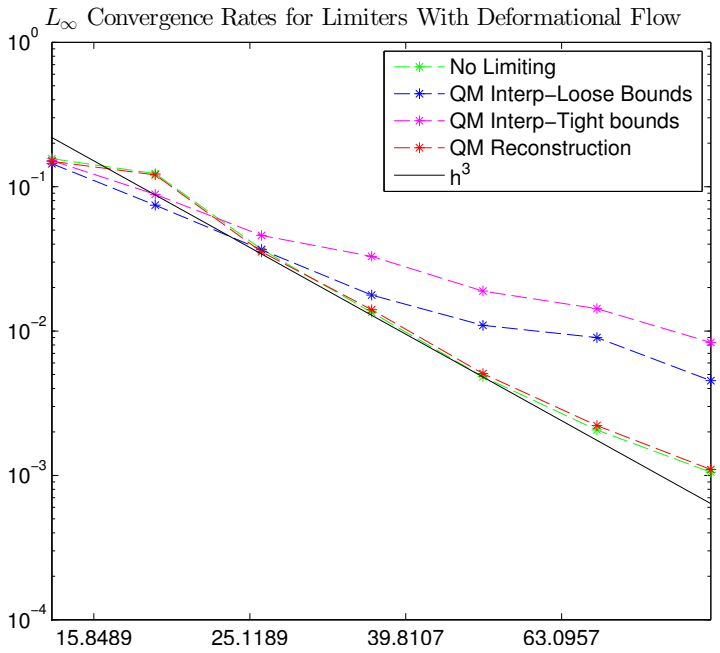

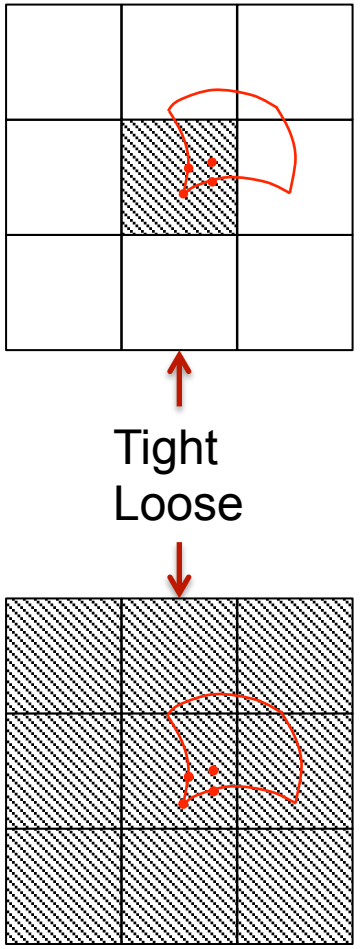

A SE+SL method with limiters would typically truncate the order of convergence to 2 even for L1 errors.

We see essentially no degradation in the 3rd order L1 error rate (compared to “raw” solution convergence).

Long-time accuracy

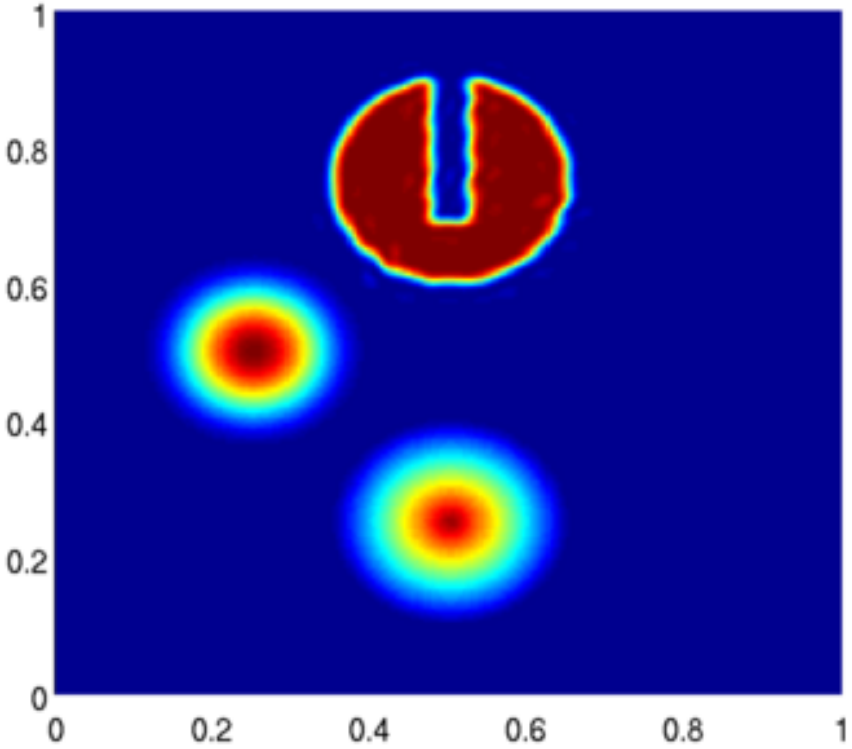

CFL=7.04

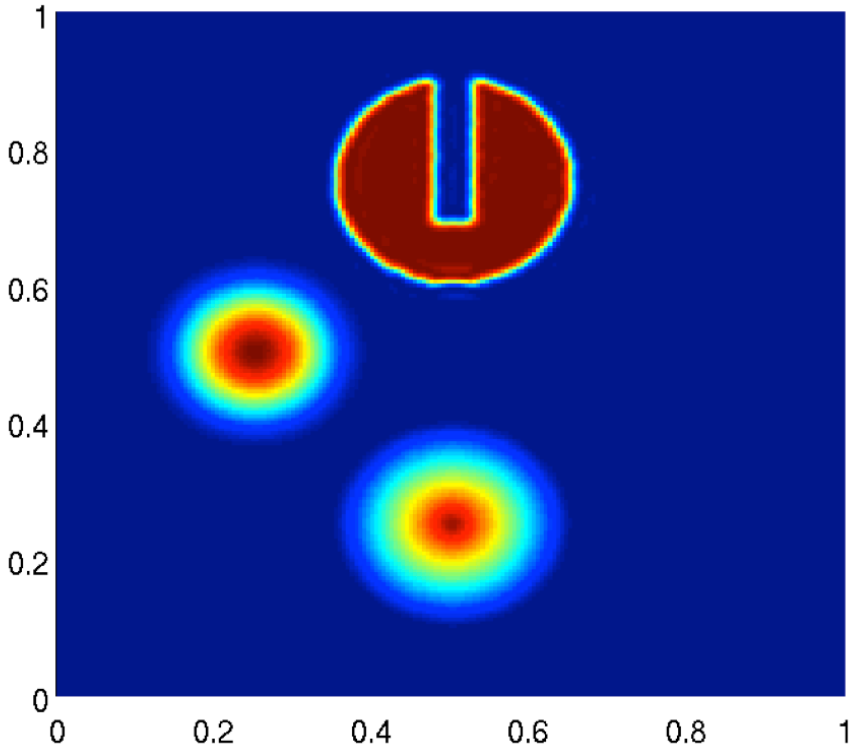

CFL=14.08

60x60 bi-cubic elements; 20 full revolutions.

Local solution bounds: $\nabla \cdot \mathbf{u} \neq 0$

Sandia National Laboratories

For $\nabla \cdot \mathbf{u} \neq 0$ the density equation is a balance rather than a conservation law.

⇒ The density is not constant along Lagrangian paths.

⇒ Taking min/max in a neighborhood of the departure points is not appropriate.

Solution: combining the Geometric Conservation Law and the balance law

$$\left.\begin{aligned} &\textbf{GC Law:} && \frac{\partial V}{\partial t} + \mathbf{u}\cdot\nabla V = V\nabla\cdot\mathbf{u} \\ &\textbf{Balance law:} && \frac{\partial \rho}{\partial t} + \mathbf{u}\cdot\nabla\rho = -\rho\nabla\cdot\mathbf{u} \end{aligned}\right\} \Rightarrow \quad \frac{\partial \rho V}{\partial t} + \mathbf{u}\cdot\nabla(\rho V) = 0 \quad \Rightarrow \quad \boxed{\frac{D(\rho V)}{Dt} = 0}$$

yields a **new conservation law** for the point "mass" distribution $M := \rho V$.

The idea is to associate and track an arbitrary initial volume V_0 and "mass" with every GLL point and use these quantities to provide bounds for the density.

Local solution bounds: $\nabla \cdot \mathbf{u} \neq 0$

Sandia National Laboratories

Assume V_n and M_n are given at t_n :

4a. Solve the GCL in $[t_n, t_{n+1}]$

$$\frac{DV}{Dt} = V \nabla \cdot \mathbf{u} \quad \text{and} \quad V(t_n) = V_n \quad \rightarrow \quad \boxed{V_{n+1} = V(t_{n+1})}$$

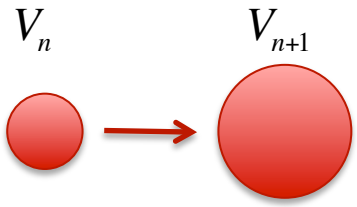

4b. Determine local bounds for the point masses:

$$M_{ij}^{\min} = \min_{\mathbf{p} \in K} M(\mathbf{p}_{ij}, t_n) \qquad M_{ij}^{\max} = \max_{\mathbf{p} \in K} M(\mathbf{p}_{ij}, t_n)$$

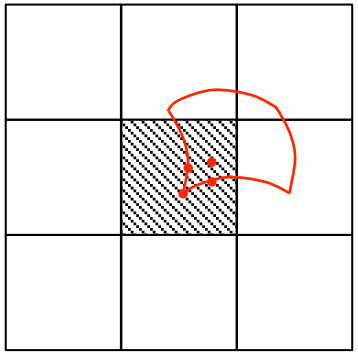

4c. Determine local bounds for the density:

$$\rho^{\min} = \frac{M^{\min}}{V_{n+1}} \qquad \rho^{\max} = \frac{M^{\max}}{V_{n+1}}$$

$$M_{ij}^{\max} = \max_{\mathbf{p} \in K} M(\mathbf{p}_{ij}, t_n)$$

$$M_{ij}^{\min} = \min_{\mathbf{p} \in K} M(\mathbf{p}_{ij}, t_n)$$

4d. Solve the mass law in $[t_n, t_{n+1}]$

$$\frac{DM}{Dt} = 0 \quad \text{and} \quad M(t_n) = M_n$$

Divergent flow

$$\mathbf{u}(\mathbf{p},t) = \begin{pmatrix} -\sin(\pi x)^2 \sin(2\pi(y-0.5))\cos(\pi(y-0.5)^2 \cos(\pi t/T) \\ \frac{1}{2}\sin(\pi x)\cos(\pi(y-0.5))^3 \cos(\pi t/T) \end{pmatrix}$$

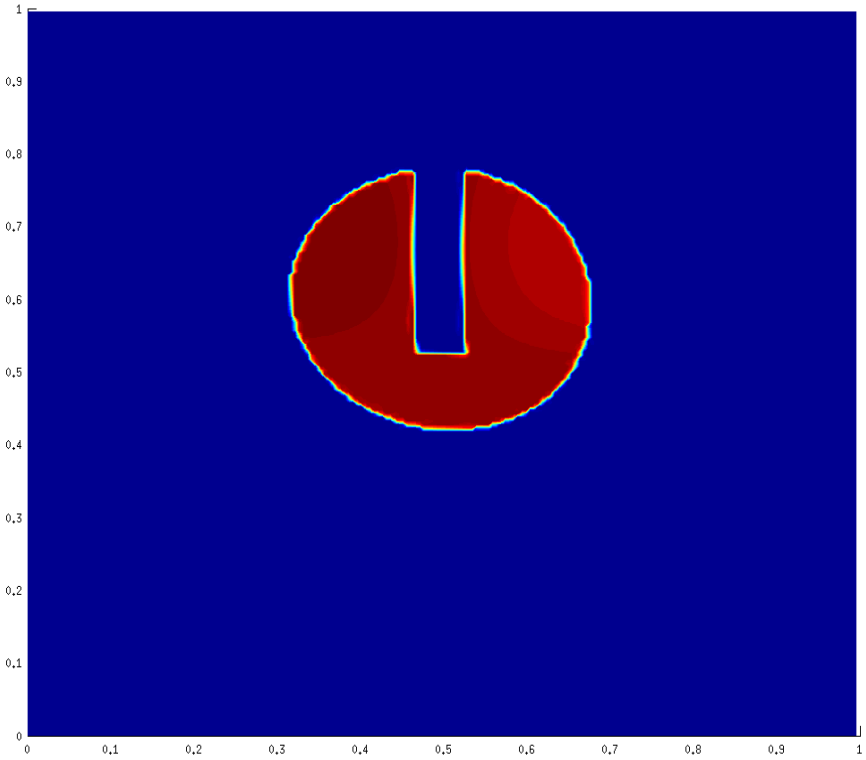

80x80 bi-cubic elements; CFL=0.7

A cell-centered semi-Lagrangian (SL) scheme

Sandia National Laboratories

Why do we care about cell-centered schemes?

- Cell-centered schemes are ubiquitous in legacy DOE codes. However,
  - These schemes use monotone reconstruction, i.e., limiters to control bounds.
  - Limiters use local "worst case" scenarios when enforcing the bounds.
  - Limiters entangle accuracy with preservation of bounds, which obscures sources of discretization errors.
- Besides getting a better scheme we will have another chance to showcase the use of optimization to preserve physical properties!

Cell-centered discretization of density and tracer

$$\mu_i = \int_{C_i} dx \quad \text{Cell area}$$

$$m_i = \int_{C_i} \rho\, dx \quad \text{Cell mass}$$

$$Q_i = \int_{C_i} \rho q\, dx \quad \text{Cell tracer}$$

$$\rho_i = \frac{m_i}{\mu_i} \quad \text{Cell average density}$$

$$q_i = \frac{Q_i}{m_i} \quad \text{Cell average tracer}$$

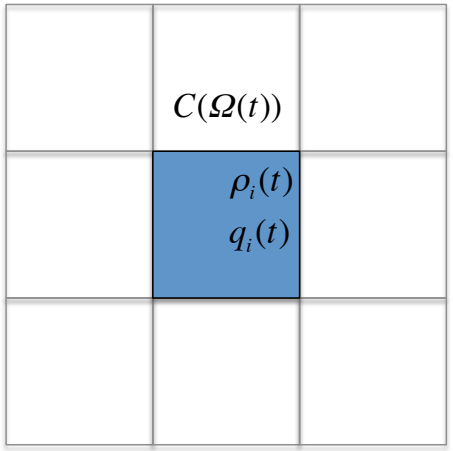

A generic cell-centered SL scheme

Sandia National Laboratories

For Lagrangian volumes

Dukowicz and Baumgardner (2000) JCP

$$\frac{d}{dt}\int_{C_i} \rho\, dx = 0 \longrightarrow m_i(t+\Delta t) = m_i(t)$$

$$\frac{d}{dt}\int_{C_i} \rho q\, dx = 0 \longrightarrow Q_i(t+\Delta t) = Q_i(t)$$

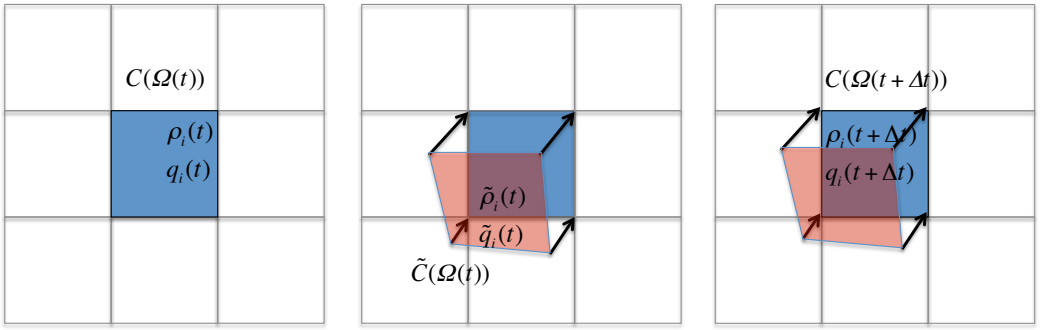

Step 1: **Trace back** cell vertices to find the Lagrangian (departure) grid $\tilde{C}(\Omega(t))$

Step 2: Remap Lagrangian quantities from arrival to departure grid:

- Reconstruct $\tilde{\rho}_i$ such that $\rho_i^{\min} \le \tilde{\rho}_i \le \rho_i^{\max}$
- Reconstruct $\tilde{q}_i$ such that $q_i^{\min} \le \tilde{q}_i \le q_i^{\max}$

$\longrightarrow$ **Lagrangian quantities**

$$\begin{cases} \tilde{m}_i = \int_{\tilde{C}_i} \tilde{\rho}_i\, dx \\ \tilde{Q}_i = \int_{\tilde{C}_i} \tilde{\rho}_i \tilde{q}_i\, dx \end{cases}$$

Step 3: **Update** values on the Eulerian (arrival) grid $\tilde{C}(\Omega(t))$

$$m_i(t+\Delta t) = \tilde{m}_i \longrightarrow \rho_i = \frac{\tilde{m}_i}{\mu_i}$$

$$Q_i(t+\Delta t) = \tilde{Q}_i \longrightarrow q_i = \frac{\tilde{Q}_i}{m_i}$$

Optimization-based low-order SL scheme

Sandia National Laboratories

Step 1: **Trace back** cell vertices to find the Lagrangian (departure) grid $\tilde{C}(\Omega(t))$

Step 2: Remap Lagrangian quantities from arrival to departure grid:

- Reconstruct $\tilde{\rho}_i$ without applying bounds
- Reconstruct $\tilde{q}_i$ without applying bounds

$\Big\} \longrightarrow$ **Lagrangian targets**

$$\begin{cases} \tilde{m}_i^T = \int_{\tilde{C}_i} \tilde{\rho}_i \, dx \\ \tilde{Q}_i^T = \int_{\tilde{C}_i} \tilde{\rho}_i \tilde{q}_i \, dx \end{cases}$$

- **Solve two quadratic programs (QP) for the Lagrangian quantities:**

$$\min_{\tilde{m}_i} \sum_{C_i} \left(\tilde{m}_i - \tilde{m}_i^T \right)^2 \quad \text{subject to}$$
$$\sum_{C_i} \tilde{m}_i = M; \quad \text{and} \quad m_i^{\min} \le \tilde{m}_i \le m_i^{\max}$$

$$\min_{\tilde{Q}_i} \sum_{C_i} \left(\tilde{Q}_i - \tilde{Q}_i^T \right)^2 \quad \text{subject to}$$
$$\sum_{C_i} \tilde{Q}_i = Q; \quad \text{and} \quad Q_i^{\min} \le \tilde{Q}_i \le Q_i^{\max}$$

Step 3: **Update** values on the Eulerian (arrival) grid $\tilde{C}(\Omega(t))$

$$m_i(t+\Delta t) = \tilde{m}_i \longrightarrow \rho_i = \frac{\tilde{m}_i}{\mu_i}$$

$$Q_i(t+\Delta t) = \tilde{Q}_i \longrightarrow q_i = \frac{\tilde{Q}_i}{m_i}$$

Advantages

- The solution is a **globally optimal state** that also satisfies the bounds:
  - By definition it is the **best possible solution** satisfying the bounds!
- The solution **provably preserves linear tracer correlations.**
- The two QPs have the exact **same structure** as in the SE-SL case:
  - We have a **fast, scalable optimization algorithm**!
  - Solution times are **essentially the same** as for conventional limiters:

Timings for Leveque's combo example.

Cells	Time steps	FCT (sec)	Van Leer	OB-SL	Ratio
64x64	400	4.51	4.55	**4.98**	**1.1**
128x128	810	47.60	48.35	**48.78**	**1.0**
256x256	1,610	390.47	399.15	**405.92**	**1.0**
512x512	3,220	5802.05	5804.66	**5655.00**	**0.9**

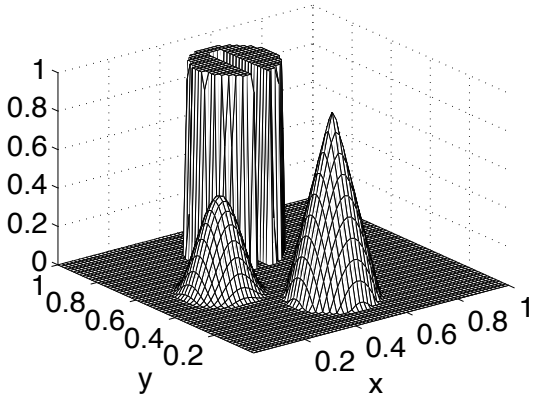

Vectorized Matlab code: **wall-clock times on a 3.06GHz Intel Core Duo MacBook Pro**

Convergence test:

Smooth Gaussian hills on a cubed sphere mesh

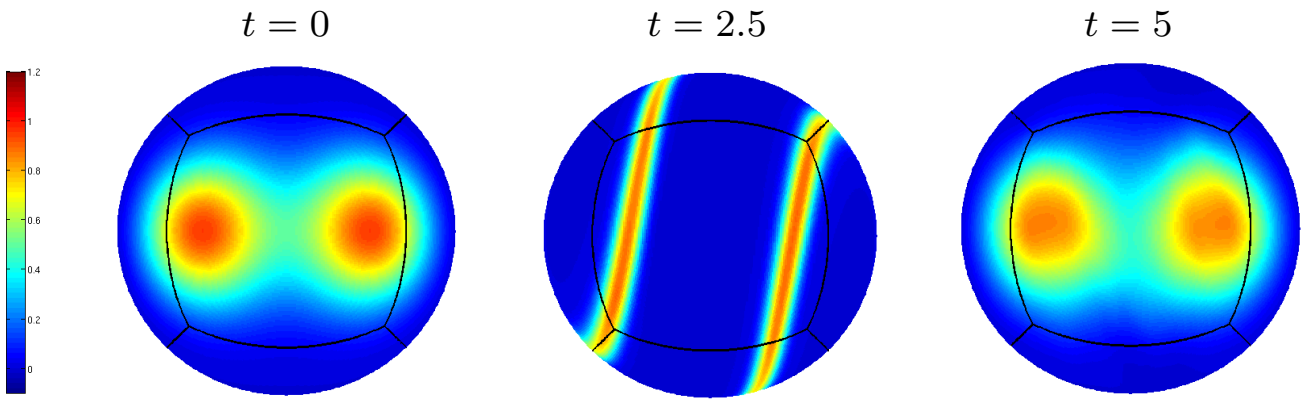

		OBT*		**Unlimited**	
mesh	steps	l_2	l_∞	l_2	l_∞
3°	600	0.386	0.465	0.368	0.425
1.5°	1200	0.182	0.268	0.172	0.225
0.75°	2400	0.0626	0.113	0.0559	0.0843
0.375°	4800	0.0167	0.0425	0.0144	0.0233
	Rate	*1.51*	*1.16*	*1.56*	*1.40*

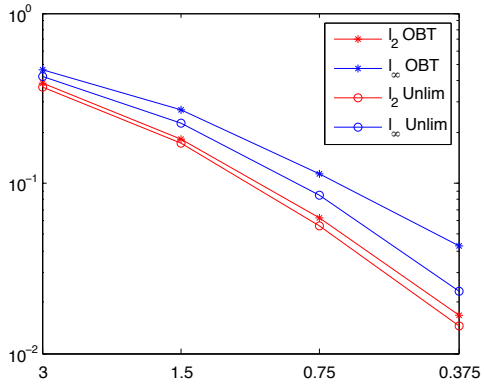

Using optimization to enforce bounds does not lead to degradation of accuracy!

Linear tracer correlations

Initial tracer distributions: two linearly correlated cosine bells

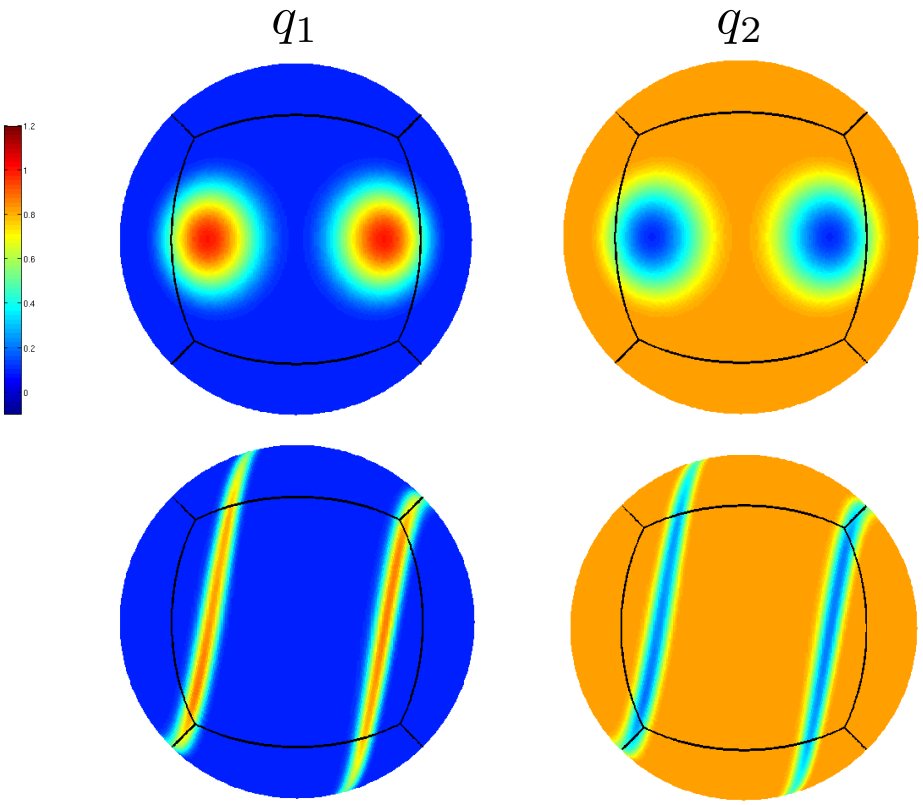

$$q_2 = -0.8q_1 + 0.9$$

Correlation $t = 2.5$

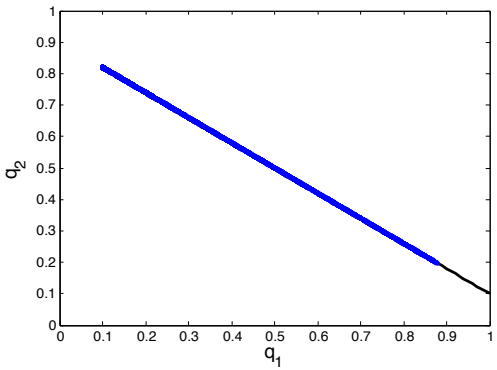

Optimization formulation provably preserves linear tracer correlations

However, …

Do you think there's anything wrong with this result?

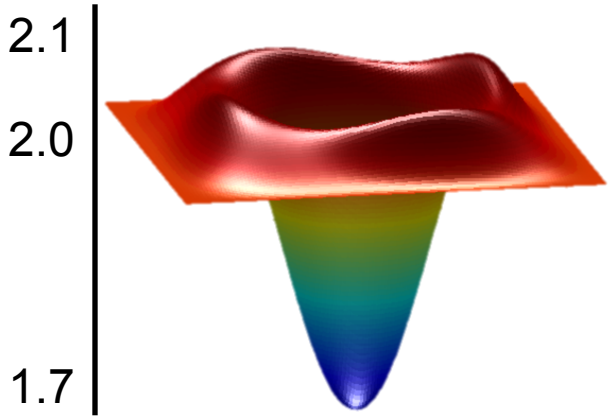

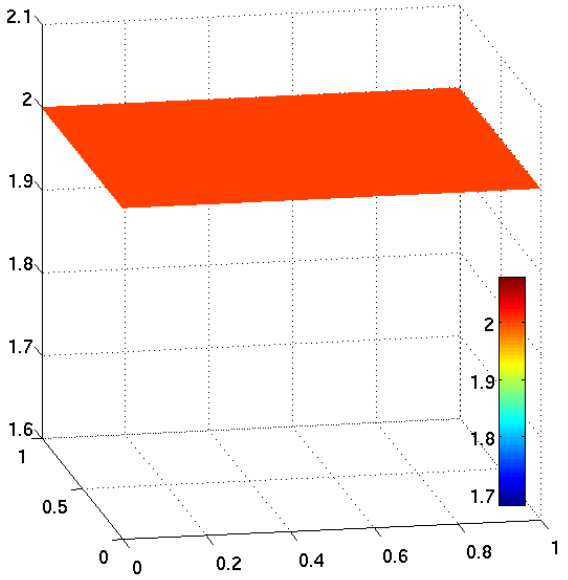

Everything! Density is supposed to be constant in time!

All we did was switch from RK4 to a forward Euler. Clearly Euler is less accurate but it is still supposed to preserve constant in time functions. So what is causing such a dramatic deterioration in the solution?

There's another physical property…

Let's take ρ=*const* and examine what happens during a single time step:

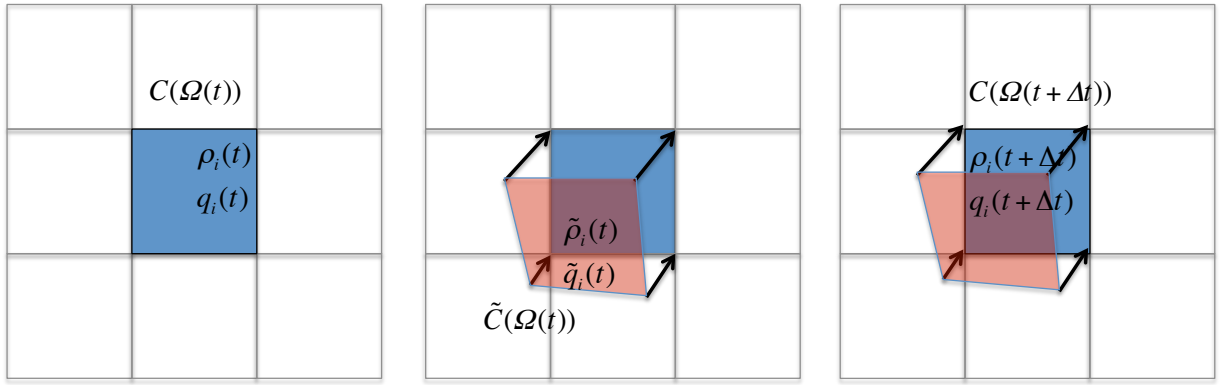

$$\rho_i(t) = \frac{m_i}{\mu_i} = \rho_{const} \qquad \tilde{\rho}_i = \rho_{const} \qquad \tilde{m}_i = \int_{\tilde{C}_i} \tilde{\rho}_i \, dx = \rho_{const} \, \tilde{\mu}_i \qquad m_i(t+\Delta t) = \tilde{m}_i \qquad \rho_i(t+\Delta t) = \frac{\tilde{m}_i}{\mu_i}$$

$$\rho_i(t+\Delta t) = \frac{\tilde{m}_i}{\mu_i} = \frac{\rho_{const}\tilde{\mu}_i}{\mu_i} = \rho_{const}\frac{\tilde{\mu}_i}{\mu_i} \neq \rho_{const}$$

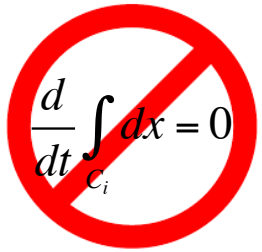

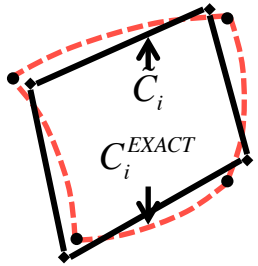

Our departure grid approximates the true Lagrangian grid, hence it violates the property that **non-divergent Lagrangian flows preserve volumes!**

The Geometric Conservation Law

Sandia National Laboratories

Our scheme violates the Geometric Conservation Law (GCL), which is critical for methods involving any kind of moving grids:

$$\frac{d}{dt}\int_{C_i(t)} dx = \int_{\partial C_i(t)} \mathbf{u}\cdot\mathbf{n}\, ds$$

Thomas, Lombardi, AIAA 17, 1979

Currently available solutions for dealing with the GCL

Use more Lagrangian points.

Lauritzen, Nair, Ullrich, A conservative semi-Lagrangian multi-tracer transport scheme on the cubed-sphere grid, JCP 229/5 (2010)

- Enforces GCL approximately.

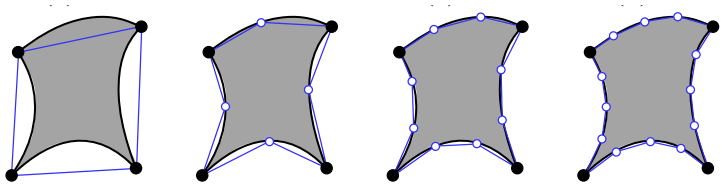

Heuristic mesh adjustment procedure:

Arbogast, Huang, A fully mass and volume conserving implementation of a characteristic method for transport problems, SISC 28 (6) (2006).

- No theoretical assurance of completion.

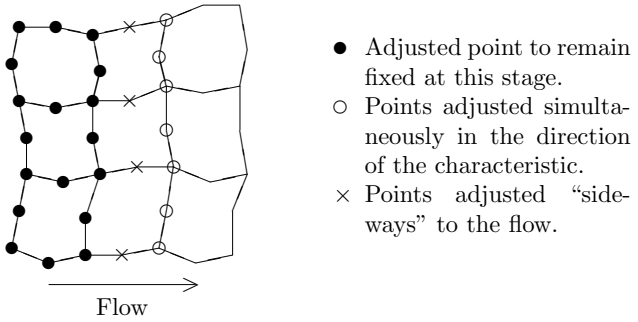

Monge-Ampere trajectory correction

Cossette, Smolarkiewicz, Charbonneau, The Monge–Ampere trajectory correction for semi-Lagrangian schemes, JCP, (2014) –

- Requires nontrivial solution of the nonlinear MAE
- Approximate: GCL ≈ accuracy of MAE scheme

Correct departure points according to

$$\tilde{\mathbf{p}}_{ij}^{corr} = \tilde{\mathbf{p}}_{ij} + (t - t_n)\nabla\phi; \quad \det\frac{\partial \mathbf{p}_{ij}^{corr}}{\partial x} = 1$$

An optimization solution to the GCL

Sandia National Laboratories

Statement of the volume correction problem

Given: source mesh $\tilde{C}(\Omega)$ and $\mathbf{c}_o \in \mathbf{R}^m$ such that $\sum_{C_i} c_{0,i} = |\Omega|$ and $c_{0,i} \geq 0 \quad \forall i$

Find: a volume compliant mesh $C(\Omega)$ such that:

a) $C(\Omega)$ has the same connectivity as the source mesh

b) The volumes of its cells match the volumes prescribed in $\boldsymbol{c}_0$

c) Every cell $C_i \in C(\Omega)$ is valid; or convex

d) Boundary points in $C(\Omega)$ correspond to boundary points in $\tilde{C}(\Omega)$

- **The volume correction problem may or may not have a solution!**
- **An important setting in which solution always exist is when**

The source mesh $\tilde{C}(\Omega)$ is transformation of another mesh $\breve{C}(\Omega)$ such that:

$$\forall \breve{C}_i \in \breve{C}(\Omega) \quad \text{is valid, or convex and} \quad |\breve{C}_i| = c_{0,i}$$

In this case $C(\Omega) = \breve{C}(\Omega)$ is a trivial solution of the volume correction problem

Volume correction as an optimization problem

We consider quads (simplices are actually easier). We need few things:

Oriented volume of a quad cell:

$$\forall C_i \in C(\Omega), \quad |C_i| = \frac{1}{2}\left((x_{i,1} - x_{i,3})(y_{i,2} - y_{i,4}) + (x_{i,2} - x_{i,4})(y_{i,3} - y_{i,1})\right)$$

Partitioning of a quad into triangles:

$$T_{i,r} \in C_i, \quad T_{i,r} = (p_{a_r}, p_{b_r}, p_{b_r}) \qquad (a_r, b_r, c_r) = \begin{cases} (1,2,4) & r = 1 \\ (2,3,4) & r = 2 \\ (1,3,4) & r = 3 \\ (1,2,3) & r = 4 \end{cases}$$

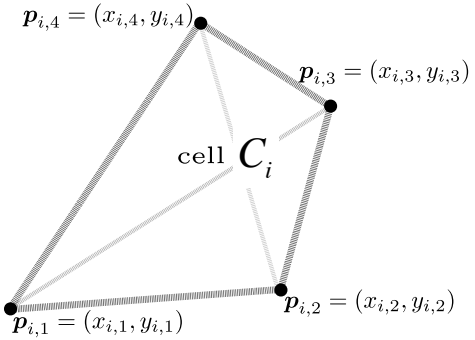

Oriented volume of a triangle

$$T_{i,r} \in C_i, \quad |T_{i,r}| = \frac{1}{2}\left(x_{i,a_r}(y_{i,c_r} - y_{i,b_r}) - x_{i,b_r}(y_{i,a_r} - y_{i,c_r}) - x_{i,c_r}(y_{i,b_r} - y_{i,a_r})\right)$$

Convexity indicator for a quad cell:

C_i is convex, if the oriented areas of all its triangles are positive: $\forall T_{i,r} \in C_i, \ |T_{i,r}| > 0$

Volume correction as an optimization problem

Optimization objective:

Mesh distance → $J_0(p,\tilde{p}) = \frac{1}{2} d(C(\Omega), \tilde{C}(\Omega))^2 = \left| p - \tilde{p} \right|_{\ell^2}^2$

Optimization constraints:

① **Volume equality** → $\forall C_i \in C(\Omega), \quad |C_i| = c_{0,i}$

② **Cell convexity** → $\forall C_i \in C(\Omega), \ \forall T_{i,r} \in C_i, \ |T_{i,r}| > 0$

③ **Boundary compliance** → $\forall p_j \in \partial\Omega, \quad \gamma(p_j) = 0$

Nonlinear programming problem (NLP)

$$p^* = \arg\min \left\{ J_0(p,\tilde{p}) \ \text{ subject to } \ (1), (2), \ \text{and } (3) \right\}$$

A simplified NLP formulation

Sandia National Laboratories

Consider a polygonal domain:

- Boundary compliance on polygonal Ω can be subsumed in the volume constraint
- Convexity can be enforced weakly by logarithmic barrier functions
- This leaves only the equality volume constraint and gives the simplified NLP:

$$p^* = \operatorname{argmin}\left\{ J(p) \;\text{ subject to }\; |C_i| = c_{0,i}\ \forall i \right\} \qquad J(p) = J_0(p) - \beta \sum_{C_i} \sum_{T_{i,r} \in C_i} \log |T_{i,r}|$$

Specialization to simplicial cells

A valid simplex is always convex ⟶ A simplex is valid if and only if $|C_i| > 0$

Since $c_{0,i} > 0$, the volume equality constraint $\forall C_i \in C(\Omega),\ |C_i| = c_{0,i}$ implies $|C_i| > 0$!

$$p^* = \operatorname{argmin}\left\{ J_0(p) \;\text{ subject to }\; |C_i| = c_{0,i}\ \forall i \right\}$$

A scalable optimization algorithm

Sandia National Laboratories

Based on the inexact trust region sequential quadratic programming (SQP) method of Ridzal and Heinkenschloss. Key properties of the inexact SQP approach:

- Fast local convergence, based on its relationship to Newton's method,
- Flexibility to use iterative ('inexact') linear systems solvers, enabling an efficient solution of very large nonlinear optimization problems.
- Key requirement in the method: design of an efficient preconditioner.

Given an optimization iterate p^k all linear systems involved are of the form

$$\begin{pmatrix} I & \nabla C(p^k)^T \\ \nabla C(p^k) & 0 \end{pmatrix} \begin{pmatrix} v^1 \\ v^v \end{pmatrix} = \begin{pmatrix} b^1 \\ b^2 \end{pmatrix}$$

$C(p^k)$ - polynomial matrix function of coordinates

Preconditioner

$$\pi^k = \begin{pmatrix} I & 0 \\ 0 & \left(\nabla C(p^k)\nabla C(p^k)^T + \varepsilon I\right)^{-1} \end{pmatrix}$$

- $\varepsilon > 0$ small parameter ~ $10^{-8}h$
- $\nabla C(p^k)\nabla C(p^k)^T + \varepsilon I$ formed explicitly
- Inverse applied using ML Trilinos (smoothed aggregation AMG)

M. Heinkenschloss, D. Ridzal, A Matrix-Free Trust-Region SQP Method for Equality Constrained Optimization, SIAM Journal on Optimization 24 (3) (2014) 1507–1541.

Applications: Lagrangian mesh motion

Sandia National Laboratories

Models the evolution of the computational mesh under a non-divergent velocity

$$\mathbf{u}(\mathbf{p},t) = \begin{pmatrix} \sin(\pi x)^2 \sin(2\pi y)\cos(\pi t/T) \\ -\sin(\pi y)^2 \sin(2\pi x)\cos(\pi t/T) \end{pmatrix}$$ ← Deformational

Rotational → $$\mathbf{u}(\mathbf{p},t) = \begin{pmatrix} 0.5 - y \\ 0.5 - x \end{pmatrix}$$

Exact | **Source (uncorrected)** | **Compliant (corrected)**

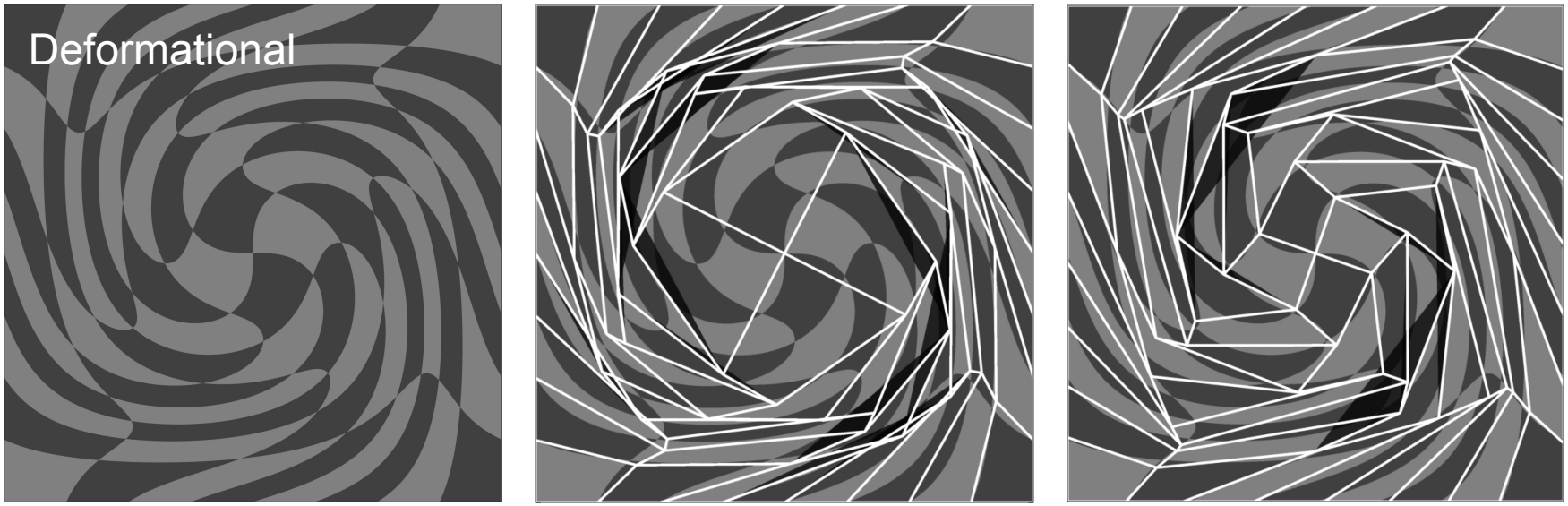

R. J. LeVeque, High-resolution conservative algorithms for advection in incompressible flow, SINUM 33 (1996)

Improvements in mesh geometry

Cell barycenters

★ - exact Lagrangian mesh

■ - source (uncorrected)

● - compliant (corrected)

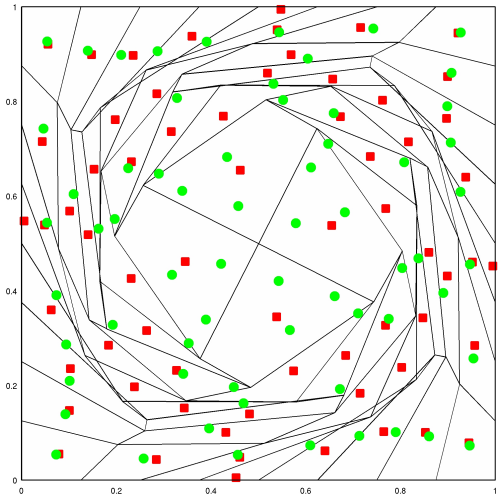

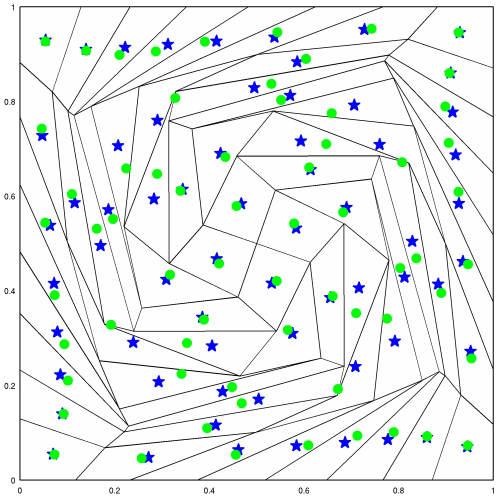

Invalid cell in the source mesh:

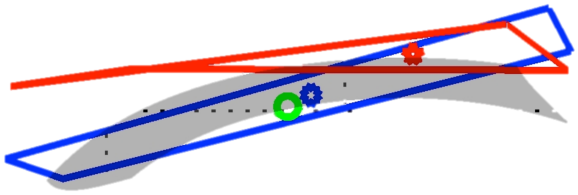

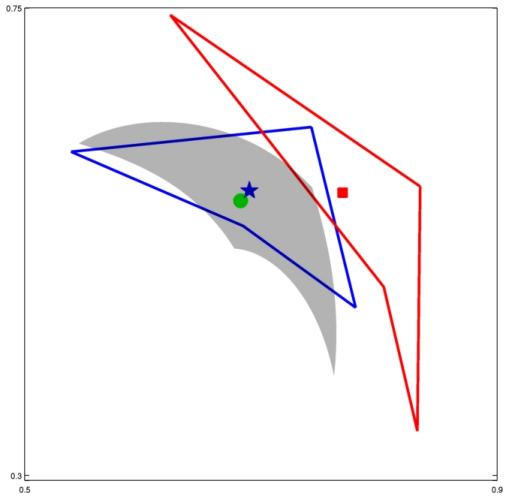

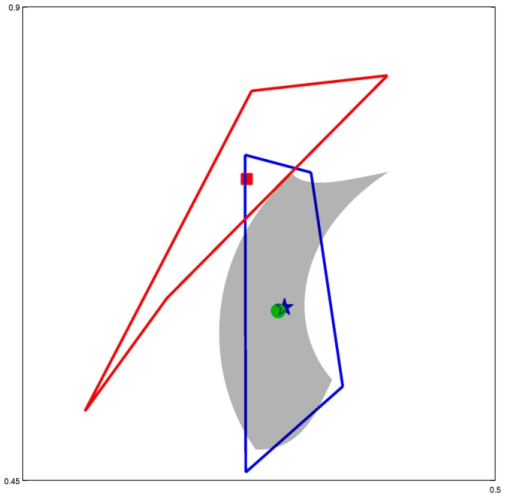

Improvements in mesh geometry

Sandia National Laboratories

Point trajectories

Rotational flow

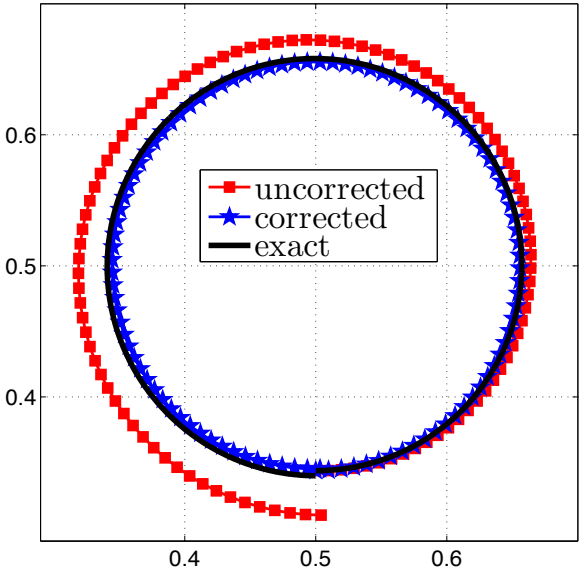

Deformational flow

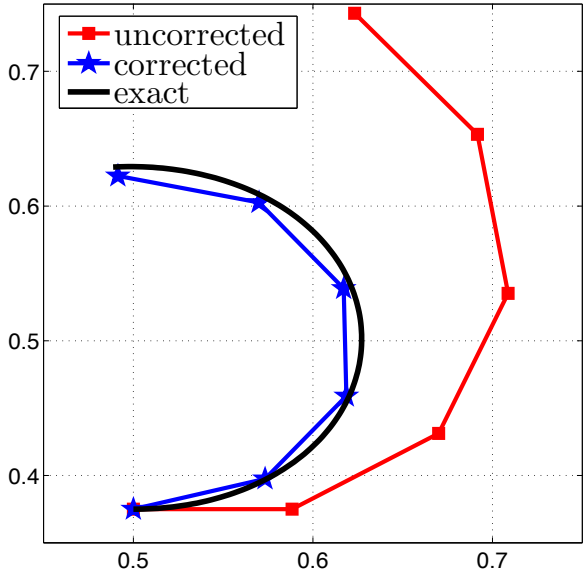

We observe significant improvements in the geometry of the corrected mesh:

- The shapes of the corrected cells are close to the exact Lagrangian shapes
- The barycenters of the corrected cells are very close to the exact barycenters
- The trajectories of the corrected points track the exact Lagrangian trajectories very closely

Applications: semi-Lagrangian transport

Sandia National Laboratories

Recall the cell-centered optimization-based semi-Lagrangian scheme:

Step 1: **Trace back** cell vertices to find the Lagrangian (departure) grid $\tilde{C}(\Omega(t))$

Step 2: Optimization-based remap of Lagrangian values from arrival to departure grid.

Step 3: **Update** values on the Eulerian (arrival) grid $\tilde{C}(\Omega(t))$

We modify it to include a volume correction step:

Step 1: **Trace back** cell vertices to find the Lagrangian (departure) grid $\tilde{C}(\Omega(t))$

Step 1$^+$: **Correct the departure grid to match the cell volumes of the arrival grid**

Step 2: Optimization-based remap of Lagrangian values from arrival to departure grid.

Step 3: **Update** values on the Eulerian (arrival) grid $\tilde{C}(\Omega(t))$

Applications: semi-Lagrangian transport

Sandia National Laboratories

Constant in time density: rotational flow

Uncorrected

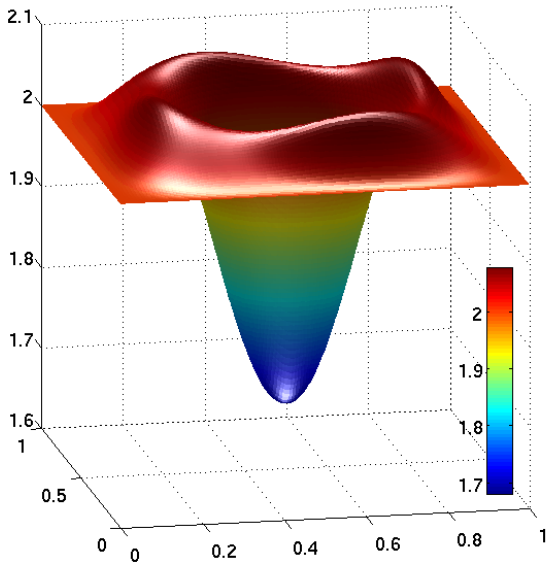

Corrected

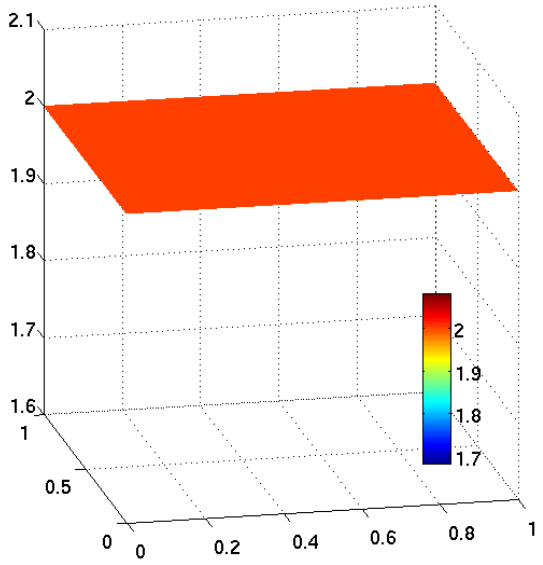

Comparison

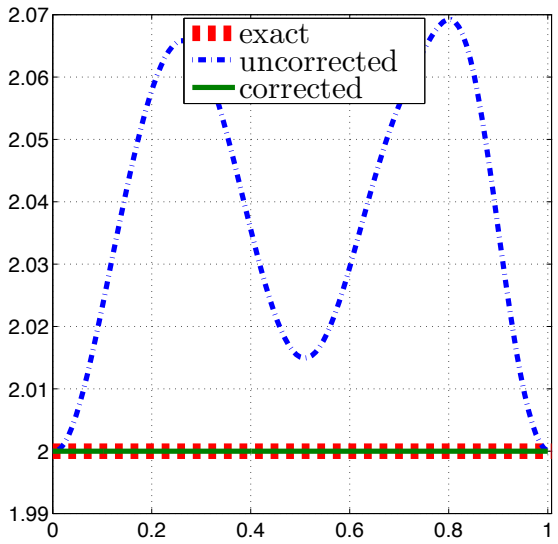

Plots of the density at time $t^N = 1.5$ for Forward Euler simulations with $\Delta t = 0.006$

Applications: semi-Lagrangian transport

Sandia National Laboratories

Initial cylindrical density distribution: rotational flow

Uncorrected

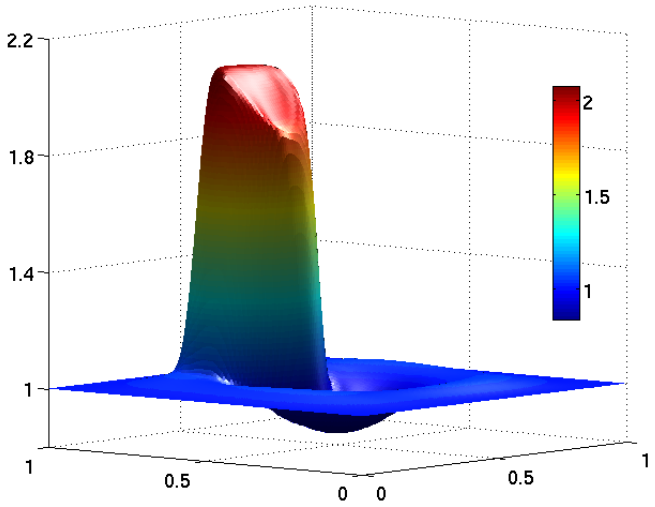

Corrected

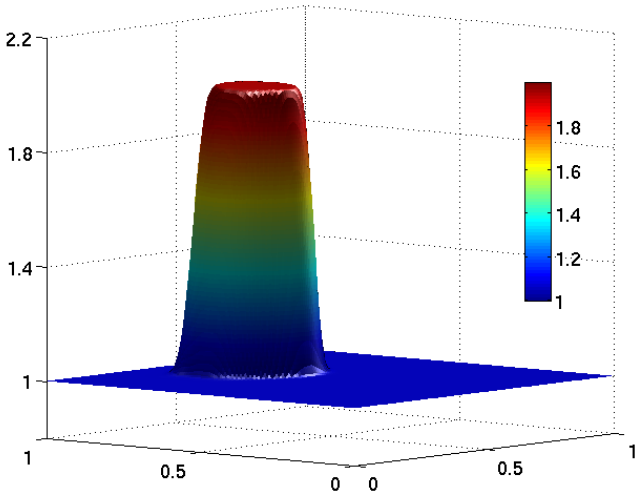

Comparison

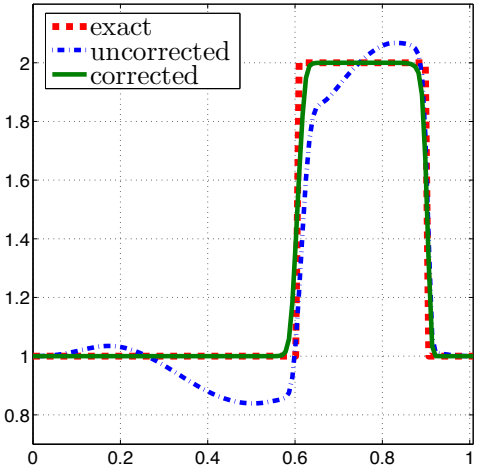

Plots of the density at time $t^N = 1.5$ for Forward Euler simulations with $\Delta t = 0.006$

Conclusions

Sandia National Laboratories

Traditional approaches to devise stable and accurate numerical methods are reaching a point of diminishing returns for complex applications involving multiple mathematical models, requiring diverse, heterogeneous numerical methods.

The use of optimization ideas to couple hetergoeneous numerical methods and to preserve the relevant physical properties is very promising

However, its success depends critically on the availability of efficient and scalable optimization algorithms to solve the resulting QPs and NLPs.

We've presented two examples where such algorithms are available and optimization leads to successful heterogenous numerical methods and property preserving schemes.